4. Injection system of the Super $c\tau$-factory

4.1. Injection into the cτ-factory

Injection into the $c\tau$-factory is carried out from the linear accelerator located in the tunnel at a height of 1200 mm from the floor. The linac tunnel floor is at the 158.82 m mark; the floor of epy technical straight section of the $c\tau$-factory is at the 162.85 m mark (in the urban coordinate system). The level difference is 4 m. The transfer line begins at a distance of +3 m from the 33rd axis of the 13th building (on the outer boundary of the lead-in tunnel).

4.1.1. Transfer line geometry

Beams are brought normally to the technical straight section of the $c\tau$-factory. Fig. 4.1 shows the electron transfer line; the positron transfer line is its symmetric reflection relative to the vertical axis of the figure. 9º bending magnet *M1X* moves the beams apart in opposite directions in a horizontal plane. Nine successive magnets M2X-M10X, lying in a horizontal plane and bending the beam through 9º, bring the injected particles to the axis of the storage ring.

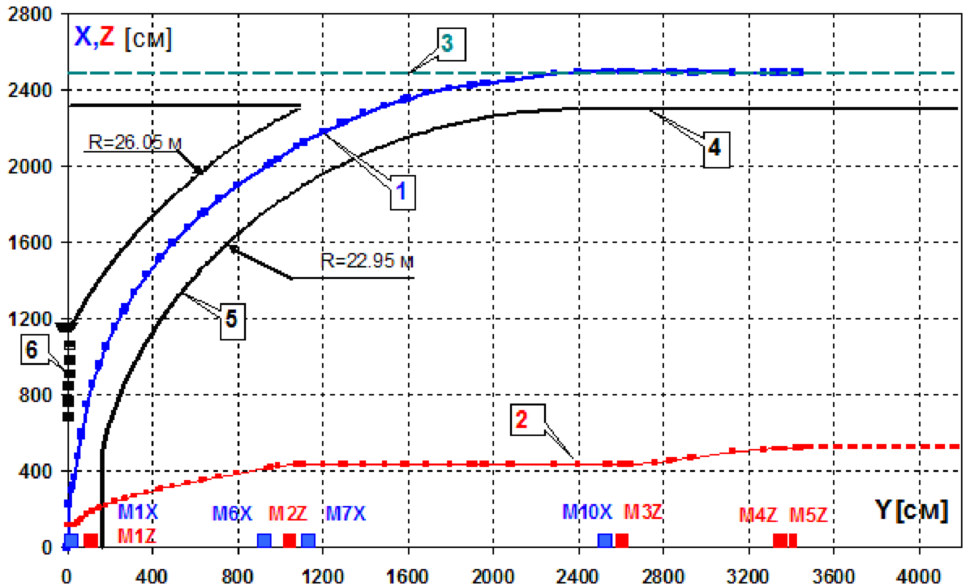

Fig. 4.1 Beam geometry in the injection line. Legend: (1) beam trajectory in horizontal, (2) beam trajectory in vertical, (3) axis of the injection (technical) straight section of the $c\tau$-factory, (4) wall of the tunnel of the technical straight section, (5) wall of the tunnel of the transfer line, (6) support columns of the injection tunnel.

Beams are elevated in the tunnel with the help of vertical magnets *M1Z-M2Z* (Fig. 4.2). The usage of magnets with a turned median plane is complicated in this case for the following reasons: (1) the floor in the elevation channel is already made under a rather large angle of 13°, (2) it is very difficult to zero the dispersion functions in horizontal and in vertical using magnets with a turned median plane, (3) oscillation coupling at injection should be minimal.

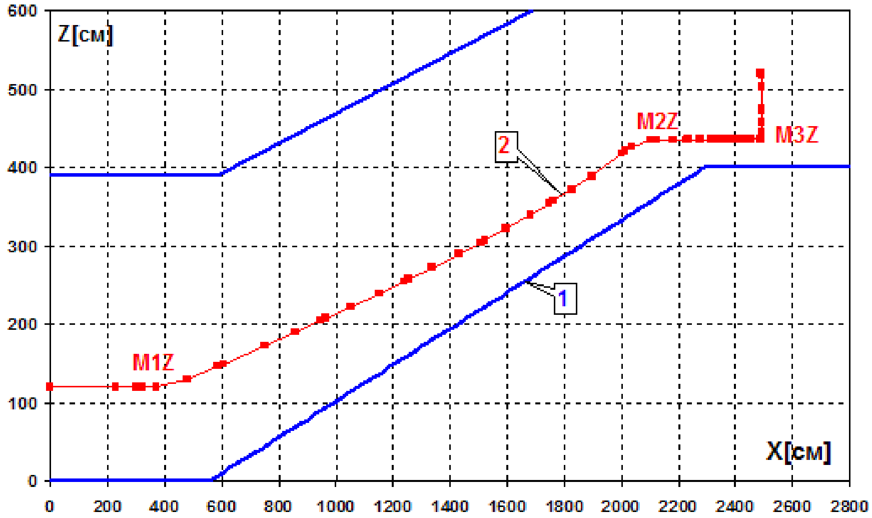

Fig. 4.2 Geometry of the elevation interval. Legend: (1) floor of the elevation channel, (2) beam axis in the vertical plane.

The beam is brought to the straight technical straight section from below and with a -800-mm vertical offset relative to the median plane of the storage ring. Then magnet *M3Z* elevates the beam in vertical and two successive magnets *M4Z* and *M5Z* bring it in the median plane at the distance ΔX = + 15 mm from the equilibrium orbit.

Magnets *M2X-M10X* and *M1Z-M3Z* are identical in design, have the effective length L = 110 cm and the maximum field H = 11.93 kG. The magnet pole width and the pole gap are tentatively assumed to be 100 mm and 16 mm, correspondingly. The pole width in magnet *M1X* is about 280 mm, in order to ensure the required field quality. Magnet *M4Z* is a septum with a current blade 30 mm thick. The length of the magnet is 144 cm, the field is 7.8 kG, and the bending angle is 7.8°. *M5Z* is a Lambertson septum magnet, with a thin magnetic blade (1 mm thick). The length of the magnet is 50 cm, the field is 3.5 kG, and the bending angle is 1.2°.

All magnets have DC supply. We have done calculations for straight magnets with edge focusing, assuming that they are made of stamped iron. However, in principle, the magnetic core of these magnets may be manufactured of solid iron, because a need to retune the field arises only when the energy of the experiment is changed.

Tentative coordinates of the injection point (in the coordinate system as in Fig. 4.2) are as follows: $X \approx 24.9$ meters (2 meters from the inner wall of the technical straight section), $Y \approx 34.4$ m (from the center of the straight interval), Z = 1.2 m (the storage rings are at this height from the floor).

БMore accurate coordinates will be obtained after the final determination of the location of the rings and channel in the tunnels.

4.1.2. Injection optics

To implement the radial and vertical achromatic bends and to match the optical functions at the inlet to the storage ring, 16 quadrupole lenses are used in each transfer line (for electrons and positrons). In addition, two lenses are placed at the entrance, in the common part, for matching with the optics of the linac.

The linear accelerator consists of modules 16 meters long. Each module comprises 4 accelerating sections, each 3 m long. Between the sections there are quadrupole lenses, creating the FODO structure as shown in Fig. 4.3.

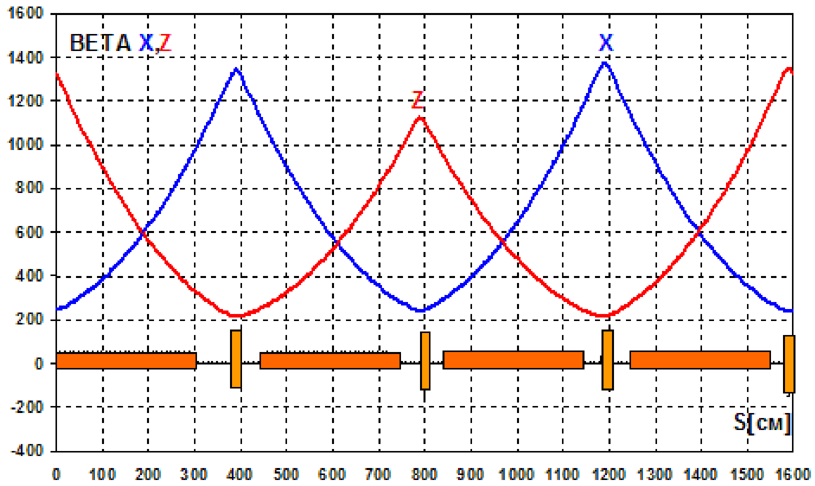

Fig. 4.3 FODO structure of the linac (a 16-meter module consisting of 4 sections and ensuring 200 MeV acceleration is shown).

Figs. 4.4 and 4.5 show the dispersion and beta functions of the transfer line.

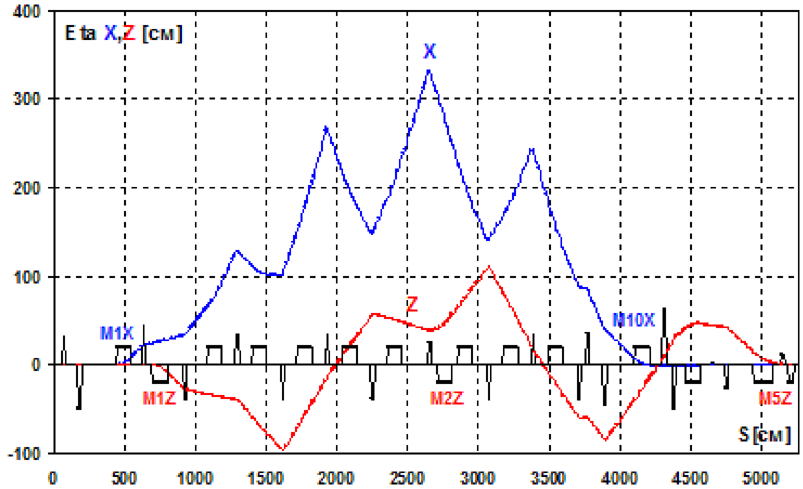

Fig. 4.4 Horizontal and vertical functions of the transfer line.

The radial injection of electrons (positrons) in the technical straight section of the $c\tau$-factory is performed using a special insert device with an increased horizontal beat function as shown in Fig.4.6.

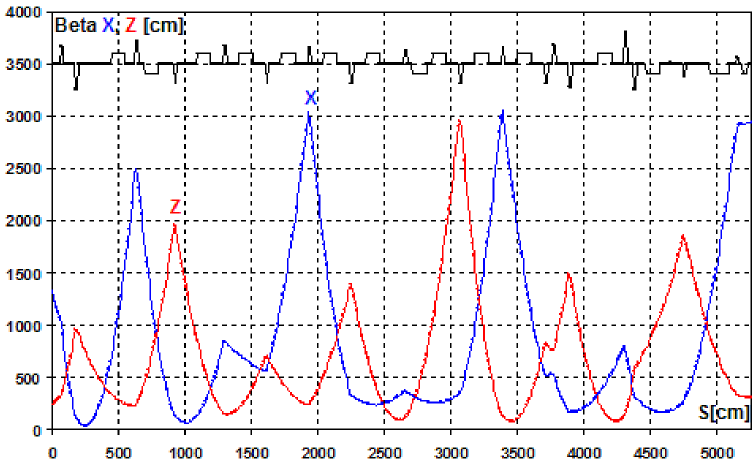

Fig. 4.5 Betatron functions of the transfer line.

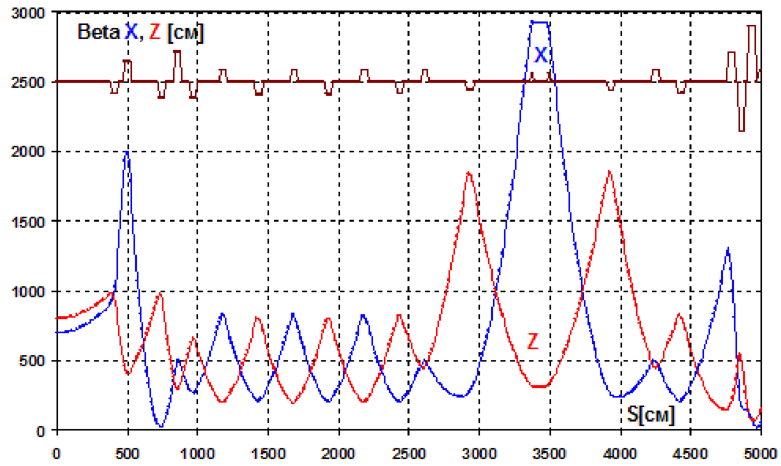

Fig. 4.6 Injection insert device in the regular structure of the technical straight section (the azimuth is ~3300 – 3500 cm).

In the injection azimuth, which is between the two focusing lenses, the betaron functions are β_x = 2940 cm and β_z = 300 cm. The horizontal betaron phase advance in the injection insert interval is $\Delta\nu_x$ = 0.65, which makes it possible to place a pre-inflector and an inflector here.

The scheme of radial injection is presented in Fig.4.7, where the parameters of the elements involved in the injection are also shown. We apply a conventional scheme using two septum magnets: *S1* with a thick ($d \approx$ 30 mm) blade and *S2* with a thin (d = 1mm) blade.

Between lenses *QF* there is a Lambertson septum magnet, which bends the beam in vertical. The small thickness of the blade of the septum magnet is achieved due to placing its yoke in the vacuum chamber of the storage ring and its coil outside. Besides, its field is rather small, H_x = 3.5 kG.

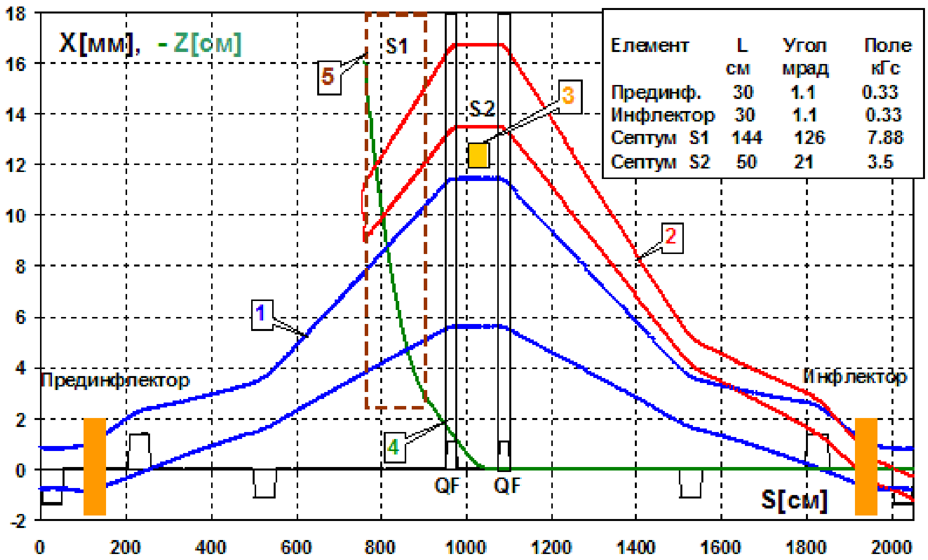

Fig. 4.7 Scheme of radial injection. Legend: (1) the stored beam after the inflector impact ($\pm 6\sigma_x$, ε_x = 8 nm-rad), (2) the injected beam ($\pm 3\sigma_x$, ε_x = 10 nm-rad), (3) the blade of second septum magnet *S2* (d =1 mm), (4) the beam trajectory in vertical at the entry, (5) the boundary of first septum magnet *S1*.

The bending angle of the magnet is chosen so that the beam vertical coordinate at the exit of *S1* be Δz > 30 mm. Septum magnet *S1* has a C-shaped yoke. The outer field coil of the magnet covers the gap and thus forms a current screen. A radial corrector is placed before septum magnet *S1* and in the focal plane of lens *QF*. The corrector deflects the beam by an angle of 2.4 mrad, so in the *S2* azimuth the injected beam has only a coordinate shift Δx = 15 mm.

For single injection of beam to the equilibrium orbit, the field in the inflector has to be increased up to H = 0.58 kG.

4.1.3. Storage ring acceptance and parameters of injected beams

The acceptances of the storage rings in vertical and in horizontal are determined by the geometrical aperture of the final focus lenses. In units of beam standard dimensions they are $A_x = 23\sigma_x$ and $A_z = 60\sigma_z$. In absolute terms, A_x = 4250 nm-rad and A_z = 180 nm-rad.

The electron beam accelerated from the photo gun to the full energy in the linac will have the following parameters: $\varepsilon_x = \varepsilon_z$ = 10 nm at E_{inj} = 1 GeV and $\varepsilon_x = \varepsilon_z$ = 5 nm at E_{inj} = 2.5 GeV; the energy spread $\sigma_E \le 1\cdot 10^{-3}$.

For the positron beam from the storage/cooler ring at the energy E = 510 MeV we have ε_x = 23 nm-rad and ε_z = 5 nm-rad. After acceleration in the linac, the emittance decreases adiabatically: ε_x = 11 nm, ε_z = 2.5 nm at E_{inj} = 1 GeV and ε_x = 4.6 nm, ε_z = 1 nm at E_{inj} = 2.5 GeV. The energy spread of positrons from the storage/cooler ring will be $\sigma_E = 5\cdot 10^{-4}$ and the bunch length at the exit from the storage ring will be σ_s = 3 mm. After acceleration in the linac at the acceleration field wavelength λ = 10 cm, the energy spread in the beam because of the bunch phase length will increase by one order. In this case, the efficiency of the capture of such beam into the storage ring of the $c\tau$-factory will not exceed 60÷70%.

To reduce the positron energy spread after the pre-acceleration in the linac, it is necessary to compress the positron bunch 2÷3 times before its injection into the linac. For this purpose it is necessary to install a section of a 15 ÷20 MeV linear accelerator in the positron extraction line, after the 90° bend. The beam energy spread will increase 4÷5 times at the exit of the section, and the bunch length will decrease after the achromaticity interval for descent to the tunnel with the longitudinal dispersion function $\eta_S \approx$ 50 cm. After these manipulations, the energy spread at the entry to the storage ring of the $c\tau$-factory will be $\sigma_E = 1\div 2\cdot 10^{-3}$, and the bunch length will be $\sigma_s \approx$ 0.5 cm (the bunch will become longer after passing the transfer line to the $c\tau$-factory, where $\eta_s \approx$ 250 cm).

4.1.4. Injection scheme and requirements to the beam parameter stability

Injection and storing take place in a radial plane. The injection point is in 34.4 from the middle of the technical straight section and between the two focusing lenses, where $\beta_x \approx$ 30 m, $\beta_z \approx$ 3 m, and $\alpha_x = \alpha_z = 0$.

The beam is brought to the lens from below. Then the Lambertson septum magnet brings the beam to the median plane in 16 cm from the equilibrium orbit (Fig.4.8). The distance between the injected beam and the stored one (after the latter has been impacted by the pre-inflector) is 6.5 mm in the azimuth of the septum magnet. The inflector puts the stored beam in the equilibrium orbit, and the injected beam experiences residual oscillations with amplitude of 6.5 mm.

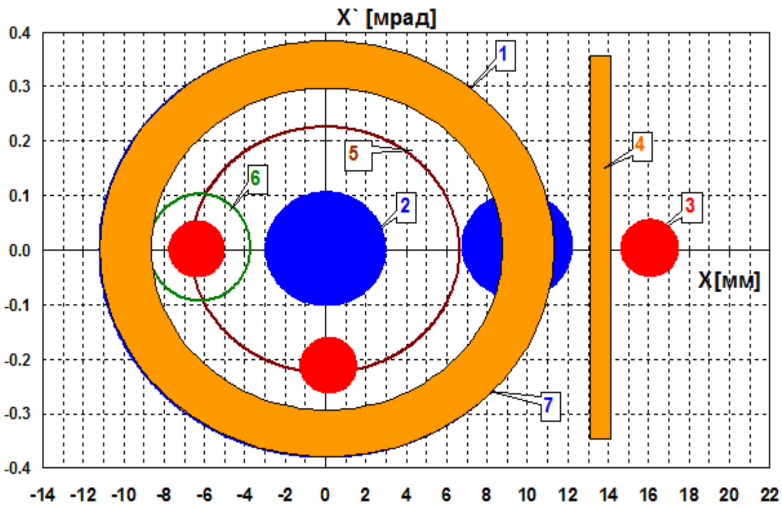

Fig. 4.8 Scheme of the radial injection and storing of beam in the $c\tau$-factory. Legend: (1) boundary of the radial acceptance of the ring A_x = 0.425 cm·mrad ($25\sigma_x$), (2) stored beam emittance, containing $6\sigma_x$ (ε_x = 8 nm), (3) injected beam, containing 95 % particles of $3\sigma_x$ (ε_x = 10 nm), (4) blade of the septum magnet (1 mm), (5) amplitude of the oscillations of injected beam after the impact from the pre-inflector (6.5 mm), (6) effective acceptance to capture the injected portion (A_{eff} = 270 nm), (7) collimator for $18\sigma_x$ (background killer) behind the inflector.

The phase advance between the pre-inflector and the septum magnet is $d\nu_x$ = 0.25; that between the inflector and the pre-inflector is $d\nu_x$ = 0.5. Ensuring a storing efficiency close to 100% imposes rather tight requirements on the vertical and horizontal position of beam at injection. From Fig.4.9, which schematically presents the efficient acceptance for beam capture and the beam itself, it follows that the requirements for a 100% injection coefficient are $\Delta x < \pm 1.5$ mm and $\Delta x' < \pm 0.04$ mrad.

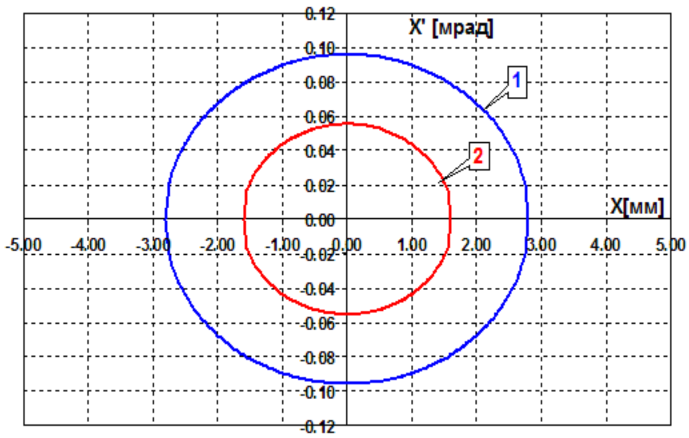

Fig. 4.9 Horizontal acceptance (A_{xeff} = 270 nm) for the injected beam (1) and the injected beam boundary containing 95% of particles for the emittance ε_x = 10 nm.

Not less stringent requirements are imposed on the position of the injected beam in vertical.

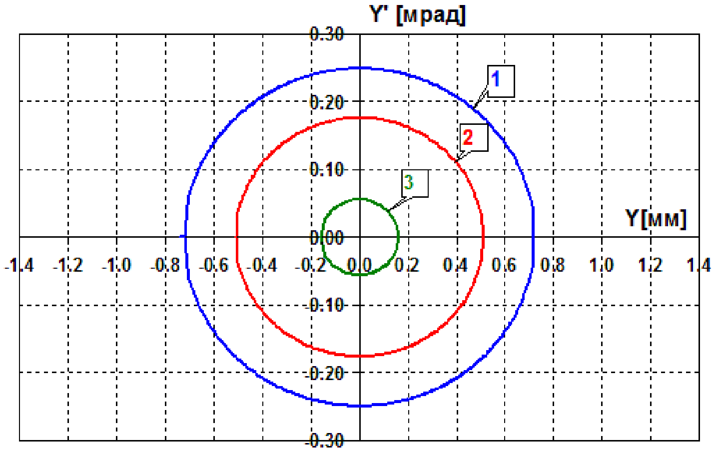

Fig. 4.10 Vertical acceptance (A_{zeff} = 180 nm, β_z = 3 m) for the injected beam (1) and the injected beam boundary, containing 95% of particles for a 100% coupling and the emittance ε_z = 10 nm.

For a 100% injection the requirements to the vertical coordinate stability and the injection angle must be as follows:

- ε_z = 10 nm $\Delta z = \pm 0.2$ mm $\Delta z' = \pm 0.075$ mrad
- ε_z = 1 nm $\Delta z = \pm 0.56$ mm, $\Delta z' = \pm 0.20$ mrad

The above requirements to the stability of the coordinate and angular position of the beam at injection allow estimating a requirement to the magnet power supply stability.

$\Delta H/H = 4\cdot 10^{-5}/1.57 = 2.5\cdot 10^{-5}$ for 90° bends. However, since these magnets are powered in series and the bends are achromatic, the power supply stability requirement decreases to about $1\div 2\cdot 10^{-4}$. For separately-powered magnets, like the 8° septum magnet with current blade, $\Delta H/H = 7.5\cdot 10^{-5}/0.139 = 5\cdot 10^{-4}$. For the inflector with $\varphi = 1.85\cdot 10^{-3}$ (at single injection), $\Delta H/H = 4\cdot 10^{-2}$.

Subject to possible simultaneous drifts, the requirements to the field stability of $\Delta H/H \leq 1 \div 2\cdot 10^{-4}$ in the permanent magnets and of $\Delta H/H \leq 1\cdot 10^{-2}$ in the pulsed inflector and pre-inflector appear quite feasible.

4.2. Polarized electron source

This project of polarized electron source is substantially based on the successful experience with such device made in the 1990s at BINP SB RAS in cooperation with the Institute of Semiconductor Physics SB RAS and NIKHEF (Amsterdam) [40, 41, 42, 43, 44]. The Amsterdam source was applied to experiments on the study of the inner structure of polarized nuclei via the scattering of polarized electrons on the nuclei of the inner target in the AmPS storage ring. Unlike the AmPS source, where a laser drew a rather long-duration electron pulse (2.1 μs, 15-50 mA, 1 Hz, polarization degree as high as 80%, 100 keV) from the photocathode, in the new source it is necessary to accelerate a single bunch of $5\cdot 10^{10} - 1\cdot 10^{11}$ electrons with a duration of 2 ns or less. Later the electron current pulse is to be compressed to an even shorter bunch suitable for direct acceleration up to energy of 2.5 GeV in a pulsed S-band linac operating with a repetition rate of 50 Hz.

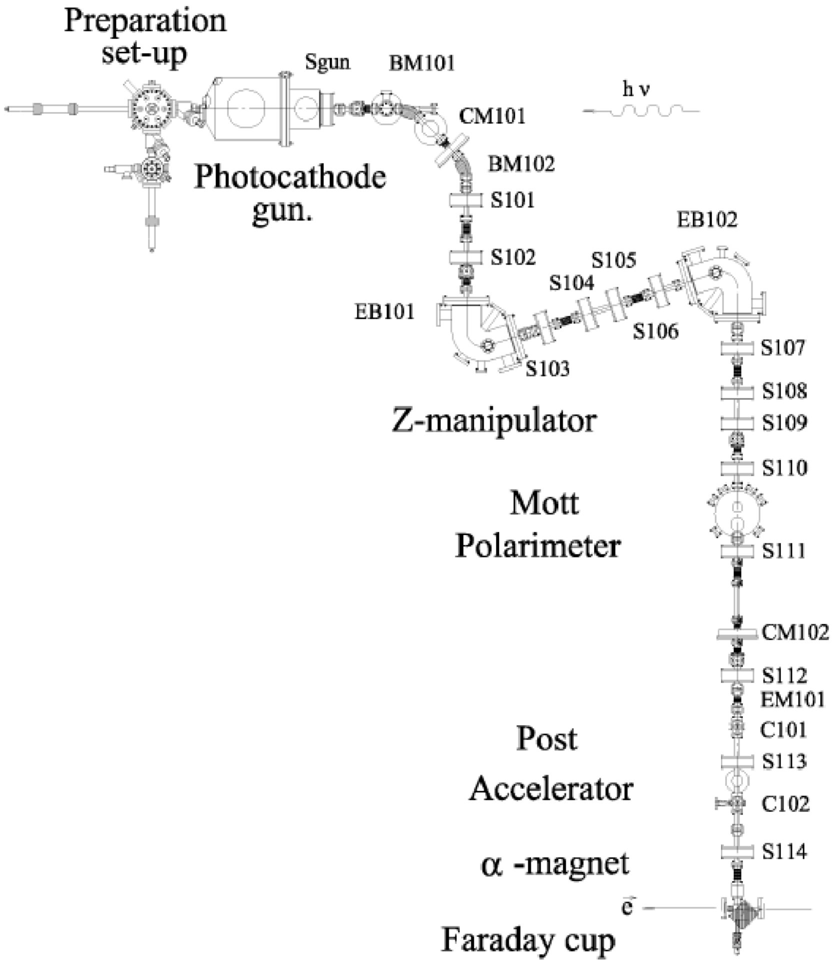

Fig. 4.11 Detailed scheme of the source of polarized electrons.

In spite of some difference in the tasks, the general arrangement of the source for the $c\tau$-factory practically repeats the AmPS source scheme (Fig.4.11). Now we proceed to the discussion of the most important units and problems of the future source.

4.2.1. Photocathode

Photocathodes in the source created for NIKHEF were structures of InGaAsP and GaAs crystalline layers [40]. Judging by our measurements, the degree of polarization was 80% in best samples. The cathodes, the system for their preparation and the laser optics were designed and manufactured at the Institute of Semiconductor Physics SB RAS at the laboratory directed by A.S. Terekhov.

In recent years, the technology of manufacturing of GaAs photocathodes used for generation of polarized electron beams has advanced significantly [45]. Almost all their options have been improved, see Table 4.1. So, the degree of electron polarization in the best photocathodes has increased up to 92% and the possibility of its further increase up to 97% has been discussed. The quantum efficiency of photocathodes has reached 0.85%.

Best photocathodes are now produced in St. Petersburg by the research team led by Professor Yu. Mamaev. These photocathodes have passed a comprehensive test at the SLAC laboratory in Stanford. They not only showed a high degree of polarization and good quantum efficiency but also demonstrated a quite acceptable lifetime. The project of the source for the ILC is also being developed on their base.

Table 4.1. Comparative characteristics of the best photocathodes [6].

Sample	Composition	P_{max}	QE(ω_{max})	Team
SLSP16	**GaAs(3.2nm)/ $GaAs_{0.68}P_{0.34}$(3.2nm)**	**92%**	**0.5%**	**Nagoya University, 2005**
SL5-777	**GaAs(1.5nm)/ $In_{0.2}Al_{0.23}Ga_{0.57}As$(3.6nm)**	**91%**	**0.14%**	**SPbSPU, 2005**
SL7-307	**$Al_{0.4}Ga_{0.6}As$(2.1nm)/ $In_{0.19}Al_{0.2}Ga_{0.57}As$(5.4nm)**	**92%**	**0.85%**	**SPbSPU, 2007**

A modern photocathode is a multilayer semiconductor structure with alternating periods of a crystal lattice grown on a relatively thick GaAs substrate. The mechanical stress induced by alloying the alternating layers of the main semiconductor with atoms of indium, aluminum and other elements creates sufficiently large splitting of the energy levels of electrons with different spin direction in the valence band. This splitting of the levels J = 3/2, m =- 3/2 and J =3/2, m =-1/2 exceeds 60 meV in the best samples, which allows rather selective emission of electrons with only one spin direction into the conduction band, Fig. 4.12 [46].

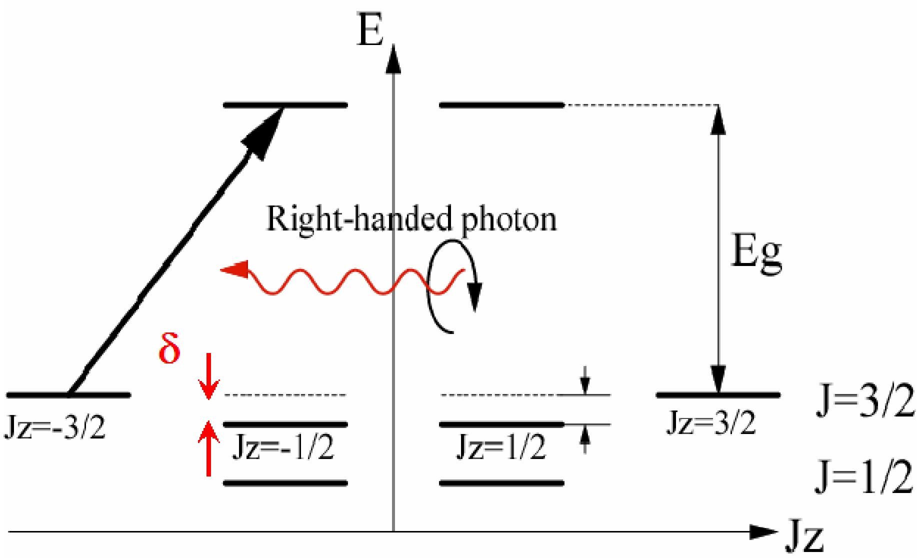

Fig. 4.12 Valence band splitting and scheme of transitions to the conductance band.

Details of the technology of photocathode preparation are outside the scope of this review. What we are interested in is the quality of this product. The graph in Fig. 4.13 shows the quantum yield and polarization vs. the wavelength of the light used [45]. One can see from the data that the maximum degree of polarization, 92%, is achieved at 825 nm.

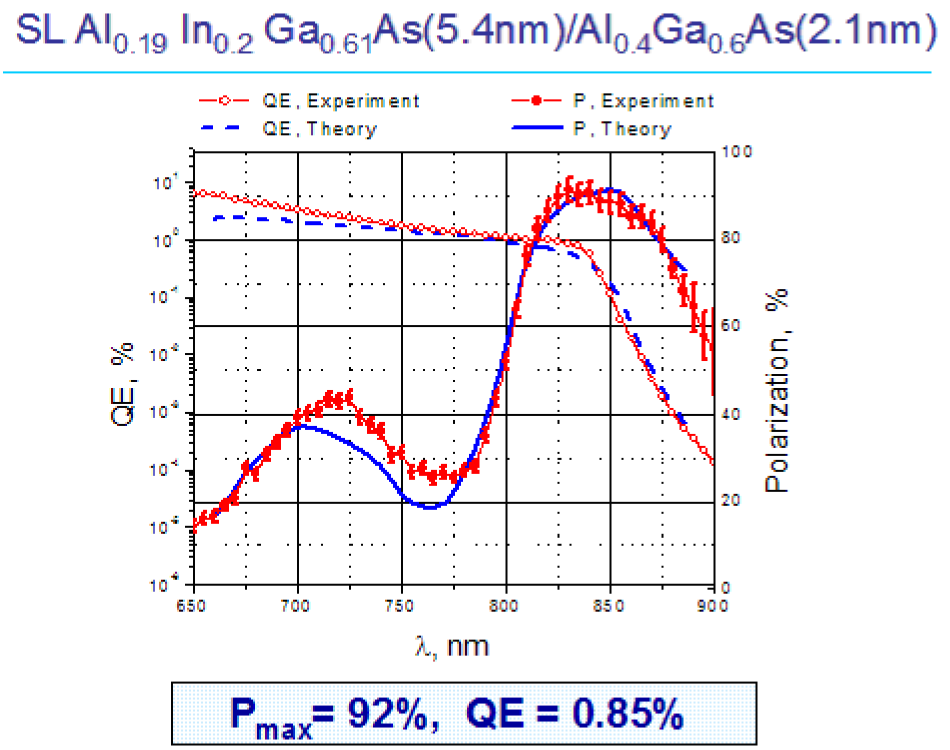

Fig. 4.13 Quantum yield and polarization degree vs. the light wavelength.

4.2.2. HV unit

The main requirement to the high voltage chamber of the photo gun is that is must ensure ultra-high vacuum, at a level of 10^{-11} mbar. The idea of using a double vacuum chamber with a 10^{-8} mbar insulating vacuum encompassing the insulators of the accelerating tube was successfully tested for the Amsterdam source. Fig. 4.14 shows a diagram of such a double vacuum chamber.

A negative voltage pulse of -100 kV about 500 microseconds in base was applied to the accelerating tube. The beam pulse duration was determined by the light flash duration. For the c-tau source, the light pulse duration should be shorter than 2 nsec.

The low pulse rate of the accelerating voltage by more than three orders of magnitude reduced the time of bombing the photocathode with dark currents, which are always present in high-voltage devices, which, in turn, allowed us to increase the lifetime of the cathodes up to one month. With a constant voltage across the accelerating gap, the lifetime of the cathode did not exceed 2-3 days.

The accelerating gap of the AmPS guns was 65 mm. The maximum field strength on the cathode surface did not exceed 17 V/cm. The photocathode diameter was equal to 12 mm, and the spot size could vary from 1 to 7 mm.

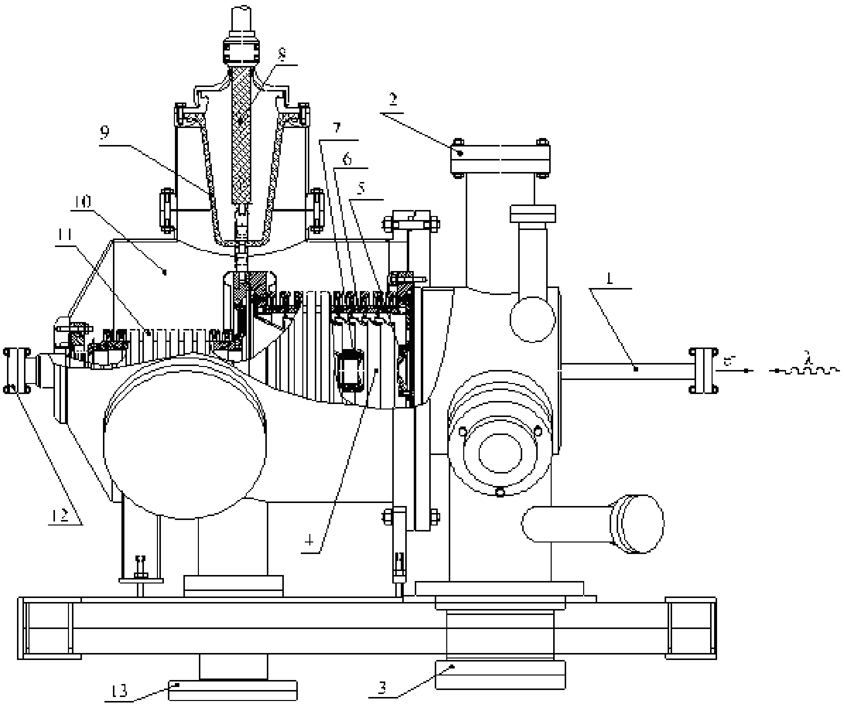

Fig. 4.14. Photo gun: 1- extraction line and the window for laser radiation input, 2,3, 13 – vacuum pumping ports, 4 – acceleration gap, 5 – anode, 8 – HV cable, 6 – insulator of the accelerating tube, 11 – second insulator of the accelerating tube, 10 – protective vacuum case, 12 – flange for interfacing the preparation and loading chambers with the unit.

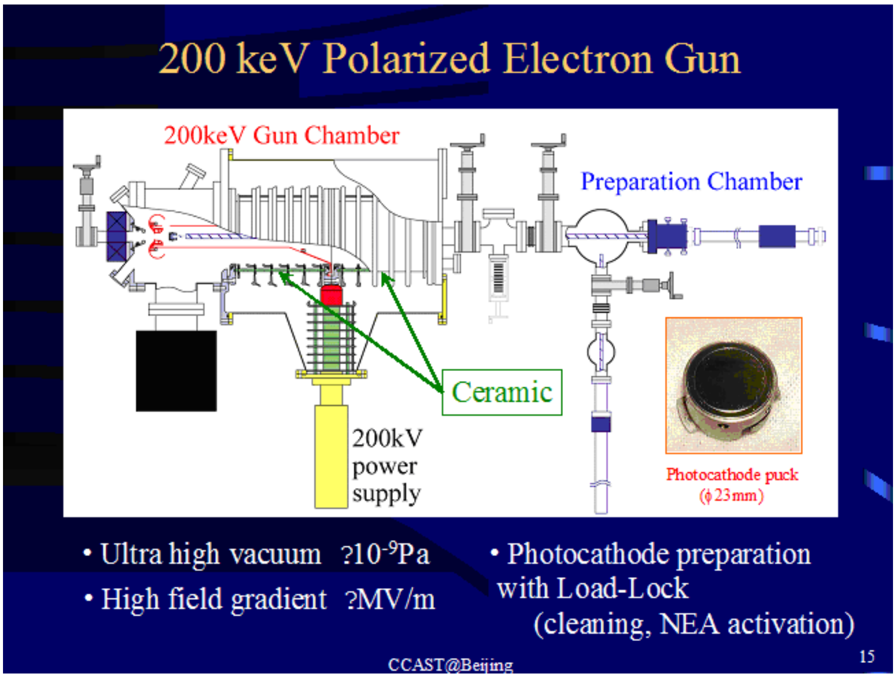

Fig. 4.15 Scheme of the HV unit of the polarized electron source for the University of Nagoya, Japan [46].

Generation of a shorter beam pulse in the c-tau source will obviously require a significantly higher rate of acceleration as compared with the AmPS source. For instance, in the source under development at the University of Nagoya within the framework of the ILC project, the acceleration rate has been increased up to 29.7 kV cm on the photocathode surface [46]. In this case, a constant accelerating voltage of -200 kV is applied to a very small gap of 35 mm,

Fig. 4.15 and Fig. 4.16. In this source, dark currents are suppressed using molybdenum as a material for the cathode electrodes and titanium as a material for the anode. Studies conducted at the University of Nagoya show the attainability of maximum field strengths of up to 1300 kV/cm for molybdenum-titanium pairs of electrodes [47]. In general, the high-voltage unit of the University of Nagoya with the preparation and loading chambers bases on the same principles that were used earlier for the AmPS source. However, the cathode in it is better screened from weak electrical discharges that occur along the ceramic insulators. Besides, magnetic lense with a longitudinal magnetic field is made as close to the photo-cathode as possible. This measure improves the matching of the beam emittance with the electron-optical path of the channel. All of these innovations as well as the new photocathodes produced in St. Petersburg will be used in the project of the source for the c-tau factory.

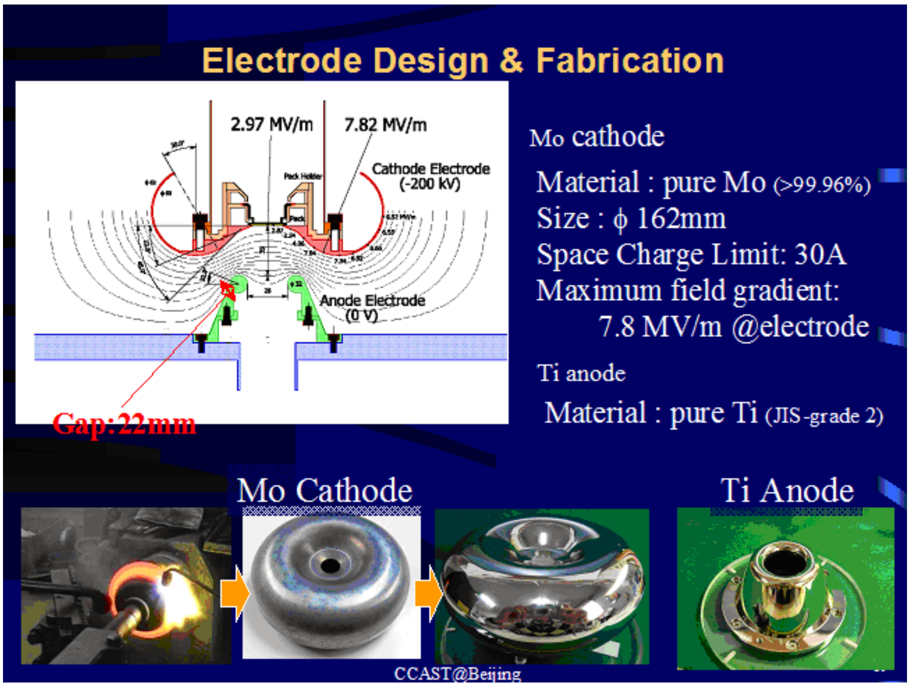

Fig. 4.16 Geometry of the acceleration interval of the source for the University of Nagoya [46].

4.2.3. Activation of the cathodes

The cathode is subjected to chemical etching in hydrochloric acid (15-20 seconds), in a nitrogen atmosphere in a fume hood. Then it is washed with methanol and dried. After that, the cathodes are inserted into frames and placed in a special sealed container on the top of the hood. The container can comprise up to three cathodes at once. The nitrogen-filled container with the cathode is transferred to the upper port of the loading chamber, also filled with pure nitrogen. Then oil-free turbo-pumps and magnetic-discharge pump out the loading chamber with the cathodes inside it to 10^{-8} mbar. After that, the cathodes are transported through a sluice to the preparation chamber, where they are placed on a carousel, up to 4 cathodes at once. The cathodes are always transported by magnetic manipulators. The chambers are separated by a gate with metal sealing.

The procedure of photo-cathode activation occurs in the preparation chamber under a vacuum of 10^{-11} mbar, maintained with an ion pump with titanium getter and NEG ribbon. The carousel is rotated, and the cathode in the frame is moved into position in front of the plate of the heater. Infrared radiation of the heater gradually warms up the cathode up to $600^0 C$. In so doing, the pressure should not rise above 10^{-8} mbar. A temperature of $600^0 C$ is maintained for one hour in order to evaporate the contaminated surface layer of different arsenic compounds. After that, the cathode is slowly cooled to room temperature.

Then, in order to reduce the potential barrier for electron emission, deposition of alternating cesium and oxygen atoms is performed. This procedure is called "Yo-Yo". The thickness of each elementary layer is about 0.1 of a monolayer. Cesium is deposited first. 12-15 pairs of layers are applied, till the saturation of the photocurrent collected on a special collector. In the process of cesium application, the cathode is continuously illuminated with a halogen lamp.

The activation over, the quantum yield is measured using a helium-neon laser at several power levels. A good InGaAsP cathode usually shows a 10-14% yield at the wavelength of this laser.

The old cathode is taken off and put to the carousel for subsequent reactivation. As a rule, 2-3 reactivations reduce the cathode quality insignificantly. The new cathode is placed on the cathode unit and tested at several wavelengths of a titanium-sapphire laser.

4.2.4. Magneto-optical system. Spin rotator

There is a lens with an axially symmetric longitudinal magnetic field set immediately at the gun exit. The configuration of the lens field is chosen in view of the influence of the space charge effect on the trajectory of the electrons. For an intense nanosecond bunch the influence of this effect must be considered and, if possible, compensated. From the results of the simulation and measurement of the normalized emittance at the University of Nagoya [46], its value does not exceed $\varepsilon_{x,y} = 10\pi \cdot mm \cdot mrad$. These measurements were made for $q = 5nC$ and a bunch duration of 1 nsec.

Then the magnetic field bends the beam through 90^0 or a slightly less angle in order to separate the light beam and the electron one. However, in principle, it seems possible to input the laser beam along an oblique trajectory, in which case no magnetic bend is required. The latter variant needs additional elaboration. Note that magnetic bends of a nonrelativistic electron beam have practically no influence on the spin, in the sense that the spin is rotated in the same way as the velocity vector.

Next, there are two ways to rotate the spin perpendicular to the velocity vector. In the Amsterdam source we used an electric field to bend the beam through 110^0. In so doing, the spin was almost not rotated and exactly perpendicular to the velocity. Then the solenoid rotated the spin around the longitudinal axis into the upright position, and the spin remained vertical after experiencing a reverse rotation by the electric field. If the solenoids between the bends were included in a configuration with a zero integral of the longitudinal field, the two electric rotations compensated each other, and the spin remained longitudinal. By adjusting the value of the longitudinal field integral, it was possible to obtain any desired orientation of the spin. This type of spin rotator is called Z-shape manipulator because of its shape in the plan.

Another variant is using the so-called Wien filter. It is a straight section with crossed electric and magnetic fields. Their effects on the velocity vector are mutually compensated, and in this case the spin is rotated around the magnetic field direction through an angle proportional to the integral of the magnetic field. The main advantage of using the Wien filter is the absence of linkage with a strictly defined energy of electrons

4.2.5. Mott polarimeter

After passing the spin rotator, the beam has a spin orientation normal to the velocity, e.g. a vertical one, see Fig.4.11. Its scattering on gold atoms through an angle of 120^0 is noticeably asymmetrical, which is usually applied to measurement of the polarization degree. Details of the polarimeter structure and particularities of its operation can be found in [41, 43].

4.2.6. Beam bunching, pre-acceleration and injection to the linac

In the AmPS source, the beam was bunched; then two cavities, which were supplied with part of the power of the 1st klystron of the large linac, accelerated it to energy of 400 keV [42]. Then the so-called alpha-magnet injected the beam to the linac axis with the help of a magnetic rotation through 270^0. Such a rotation has several advantages as compared with rotation through 90^0. It can be made achromatic and focusing in both transverse coordinates. In addition, it has a certain bunching effect, which is opposite in sign to the drift gap. In the version with unpolarized electron source, the alpha-magnet was turned off to pass the beam from the straight direction.

4.2.7. Main parameters

In conclusion, Table 4.2 presents a list of the main subsystems of the polarized electron source.

Table.4.1 Main subsystems of the polarized electron source.

Glove box for photocathode etching
Loading chamber
Preparation chamber
Magnetic manipulators
Photo gun + 100 kV pulsed power supply (0.2 ms pulse, 50 Hz)
Ultra-high vacuum system (pumps, heaters, NEG, sensors): $p < 10^{-11}$ mbar
Ti-Sapphire drive laser + optics
Z-shape spin-manipulator
100 keV beam line
Mott polarimeter
Sub-harmonic pre-buncher + pre-accelerator
Alpha-magnet
Faraday cup

The main design parameters of the source of polarized electrons for the c-tau factory are shown in Table 4.3. It should be noted that many of the characteristics of the beam are determined not so much by the photo gun quality as such but by its subsequent transformation in the process of bunching and pre-acceleration. In particular, the value of emittance is not reliably predictable at this stage.

Table.4.2 Parameters of the source of polarized electrons for the c-tau factory.

Beam polarization	80-90%
Polarization lifetime in ring	3000-4500 s
Cathode voltage (pulsed, 02 ms, 50 Hz)	-100 kV
Photocathode type	AlInGaAS/AlGaAS SL with strained QW, SPbSPU
Laser type	Ti-Sapphire
Laser wavelength	700-850 nm
Laser energy in pulse	10 mkJ

Pulse duration	2 ns
Repetition rate	50 Hz
Number of electrons/pulse	3×10^{10} (5 nC)
Normalized beam emittance, rms	10-30 mm-mrad
Photocathode quantum efficiency	up to 0.5 %
Photocathode recesiation time	200-600 hours (depends on laser power)

4.3. Production of intense positron beams at the injection complex

4.3.1. Introduction

There are two processes known to be practically suitable for production of positrons: (a) β+ decay of radioactive isotopes and (b) production of electron-positron pairs when a relativistic photon passes in the field of atom nucleus. Positron sources based on the β+ decay are not well suited for experiments with colliding electron-positron beams because of the relatively low intensity of particle production as well as the complexity of the collection of produced positrons into short narrowly focused bunches the modern accelerators work with. In the accelerator technology, the process of production of electron-positron pairs in an electromagnetic shower is used for the production of positrons. An electromagnetic shower can be obtained via directing a high-energy electron beam on a target. Electrons lose their energy in the target and emit relativistic bremsstrahlung photons. These photons produce high-energy electron-positron pairs in the field of the nuclei, which pairs emit new photons. The avalanche multiplication of particles occurs until the electrons and positrons slow down so that the energy loss due to bremsstrahlung equals the ionization losses. This critical energy for different substances can be roughly estimated by the formula [30, p. 213]

$$E_c = \frac{800\ МэВ}{\mathrm{Z}+1.2}, \tag{4.1}$$

where Z is the number of protons in an atom of the material of the target.

Modern positron sources based on particle production in electromagnetic shower [1, 2] operate on a principle which was first implemented in Stanford in the 1950s [3]. Fig. 4.17 shows the general scheme of such a source. The electron beam of linear accelerator, focused on a target of a material with a high atomic number, generates an electromagnetic shower. Shower-produced positrons leave the target with a large angular and energy spread (Figure 4.18), so only a small fraction (typically <10%) of these particles can be focused and accelerated in the second linear accelerator. The beginning of this accelerator is placed in a solenoidal magnetic field that ensures retention of positrons near the axis of the accelerating structure until they acquire a longitudinal momentum sufficient for using quadrupole lenses for alternate-sign focusing in the rest of the accelerator.

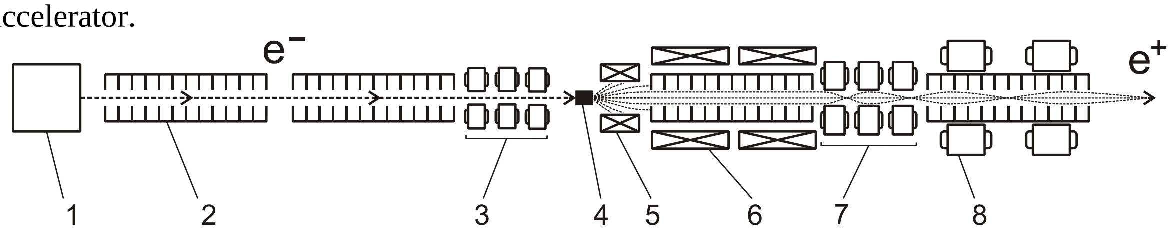

Fig. 4.17. Scheme of a typical source of positrons for the acceleration technology. 1 — electron source, 2 — accelerating RF structure, 3 — quadrupole lenses focusing electrons on the target, 4 — conversion target, 5 — the matching device, 6 — solenoid comprising the first structure for positron acceleration, 7, 8 — quadrupole lenses.

The number of positrons in the maximum of the electromagnetic shower produced by an electron with energy E is given by the following expression [9, p. 197]:

$$N_{e^+} \approx \frac{0{,}15}{\sqrt{\ln(E/E_c) - 0{,}37}} \cdot \frac{E}{E_c}, \tag{4.2}$$

This dependence is close to linear for a broad energy range (see Fig.4.9), that is why the positron source efficiency is usually measured with the following value:

$$Y = \frac{1}{E} \cdot \frac{N_+}{N_-}, \tag{4.3}$$

which is called the positron yield. Here N_- is the number of positrons coming to the target; N_+ is the number of accelerated positrons. Modern facilities give the positron yield $Y = 0{,}02 \div 0{,}06$ GeV^{-1} (see Table 4.3).

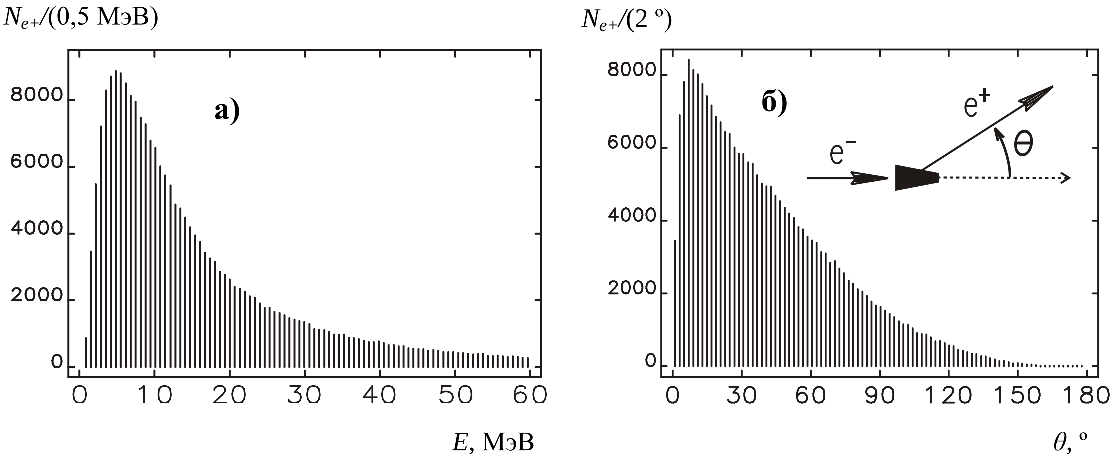

Fig. 4.18. Energy (a) and angular (b) spread of positrons coming out of the conversion target. The spectra were obtained using the GEANT code [16] (the number of electrons coming to the target is $2 \cdot 10^5$; the electron energy is 280 MeV; the tantalum target length is 12 mm). The total number of positrons coming out of the target is $2{,}4 \cdot 10^5$ (the disagreement with the formula is explained by the fact that approximately half of the shower-produced positrons annihilate inside the target). The spectra are in weak dependence on the primary electron beam.

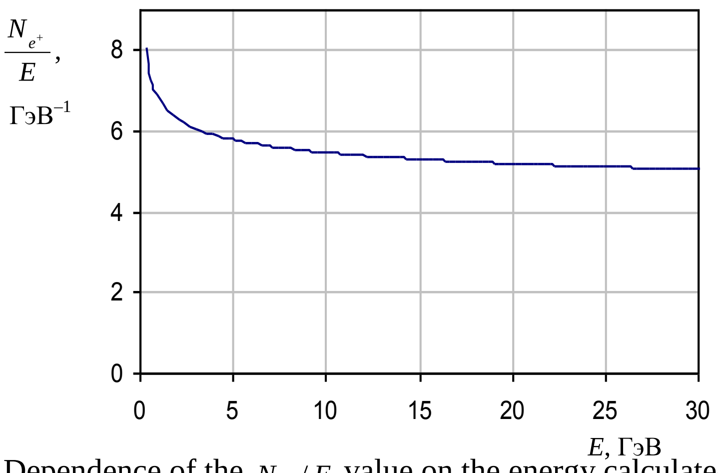

Fig. 4.19. Dependence of the N_{e^+}/E value on the energy calculated by formula (4.2).

Table 4.3. Parameters of the positron sources. Abbreviations: flux concentrator (FC) and quarter-wave transformer (QWT). Parameters that were not found in literature and thus were calculated from indirect data are marked with asterisk.

Facility name	PEP-II	KEKB	DAFNE	BEPC	DORIS	LIL
Research center	SLAC	KEK	LNF	IHEP	DESY	CERN
Country	USA	Japan	Italy	China	Germany	Switzerland
Frequency of the accelerating RF structures, MHZ	2856	2856	2856	2856	2998	2998
Frequency of the complex, Hz	120	50	50	12.5	50	100
Energy of e^- on the target, GeV	33	3.7	0.19	0.14	0.4	0.2
e^- per bunch	$5\cdot10^{10}$	$6\cdot10^{10}$	$1.2\cdot10^{10}$*	$5.4\cdot10^{9}$*	$3.1\cdot10^{9}$*	$3\cdot10^{9}$*
Field in the solenoid, T	0.5	0.4	0.5	0.35	0.4	0.36
e+ energy after solenoid, MeV	120	100	120*	100		90
Material of the target	W-25Re	W	W-25Re	W	W	W
Type of the matching device	FC	QWT	FC	FC	QWT	QWT
Parameters of matching device	B = 6 T L = 10 cm	B = 2 T L = 4.5 cm	B = 5 T L = 12 cm	B = 2.6 T L =12 cm	B = 1.8 T L = 4.5 cm	B = 0.83 T L = 4.4 cm
Positron yield after the linac, 1/GeV	0.054*	0.023	0.053	0.014	0.025	0.0295
Energy of the storage ring, GeV	1.15	3.5	0.51	1.3	0.45	0.5
Energy acceptance of the storage ring, (ΔE/E) ·100%	2 %	0.5 %	3%	1%	1%	2 %
Positron production, 1/s	~$8\cdot10^{12}$*	~10^{11}* ($2\cdot10^{11}$*)	~$2\cdot10^{10}$*	~$2.5\cdot10^{8}$*		~$2.2\cdot10^{10}$*
Information sources	[17, 18, 19]	[20, 21]	[22, 23, 24]	[25, 26]	[27, 28]	[27, 29]

The VEPP-5 injection complex is intended to provide relativistic electrons and positrons for elementary particle physics experiments on colliding electron-positron beams. Particular attention in the development of the positron source was placed on the magnetic system for collection of positrons after the conversion target. As a result, a pulsed axial magnetic lens with magnetic field of fairly high quality (with a small field transverse component deflecting the particles from the accelerator axis) was created, which ensured a fairly high positron yield ($Y \approx 0{,}1$ GeV^{-1}) of the positron source at a relatively modest cost of the installation construction. The BINP-developed source allows producing $5\cdot10^{8}$ positrons in one pulse.

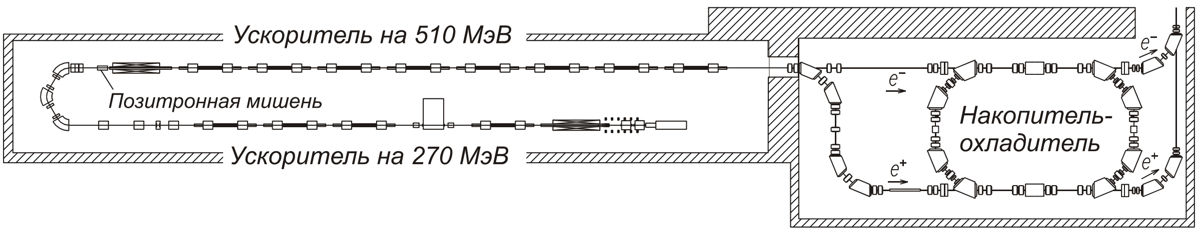

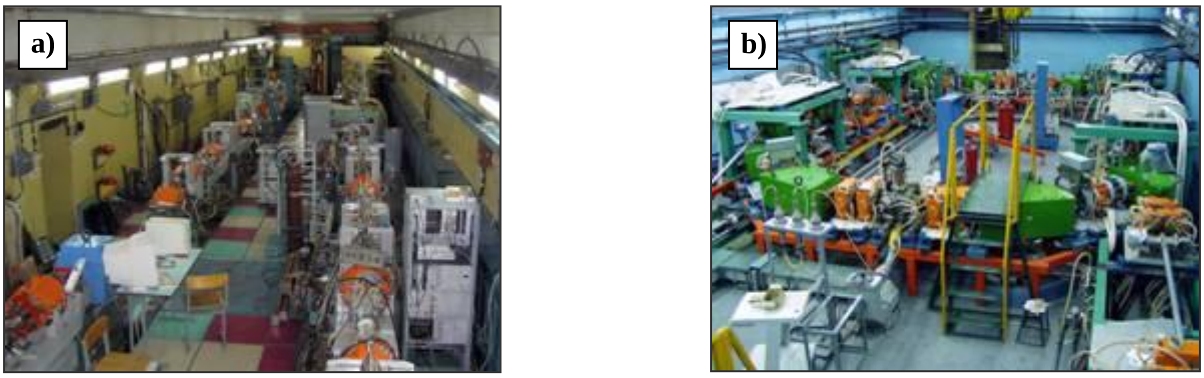

Fig. 4.20. VEPP-5 injection complex. a) linear accelerators, b) storage/cooler ring.

These positrons are accelerated to energy of 70 MeV in the first accelerating section after the target. The electron beam coming to the target contains $2\cdot10^{10}$ electrons with energy of 270 MeV.

Table 4.4. Design objectives for the pre-injector

Final energy of beams	510 MeV
Electrons per pulse	$2\cdot10^{10}$ e^-
Positrons per pulse	$5\cdot10^{8}$ e^+
Pulse repetition rate	50 Hz
Energy spread of	
electron beam	± 1 %
positron beam	± 3 %
Emittance of	
electron beam	~ 10^{-5} rad·cm
positron beam	~ 10^{-4} rad·cm
Working radio frequency	2856 MHz
Pulse power of klystron	≈ 60 MW
Number of klystrons	4 pcs.
Total power consumption	600 kW

Table 4.5. Design objectives for the storage/cooler ring

Beam energy	510 MeV
Perimeter	2740 cm
Radio frequency	700 MHz
Time of radiation damping	18 ms (τ_z)
Beam output parameters	
number of particles	$2\cdot10^{10}$ e^+ or e^-
energy spread	± 0,07 %
longitudinal size	4 mm (σ_z)
horizontal emittance	$2{,}3\cdot10^{-6}$ rad·cm
vertical emittance	$0{,}5\cdot10^{-6}$ rad·cm
Total power consumption	800 kW

4.3.2. VEPP-5 injection complex

The VEPP-5 injection complex (Fig.4.20) is a modern source of relativistic electrons and positrons under construction at Budker Institute of Nuclear Physics for operation of facilities on colliding electron-positron beams. The basis of the injection complex is the pre-injector, i.e. two linear accelerators for energy of 270 MeV and 510 MeV. After rotation through 180° in a magnetic field, electrons from the first accelerator come to the conversion target and produce positrons, some of which are then accelerated up to 510 MeV in the second accelerator. A pre-injector operation mode in which only electrons are accelerated is also possible. In this case, individual electron bunches are sent past the target to the second linear accelerator, which is arranged so that to accelerate electrons from 270 MeV to 510 MeV.

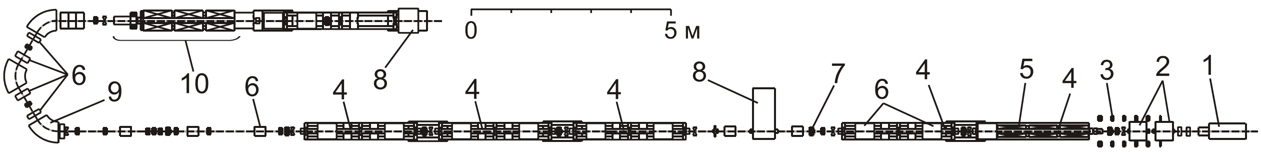

Fig. 4.21. Scheme of the positron injection source of the VEPP-5 complex. 1 — electron gun, 2 — subharmonic buncher, 3 — focusing coil, 4 — acceleration structure, 5 — solenoid coil, 6 — quadrupole lens, 7 — corrector, 8 — spectrometer, 9 — bending magnet, 10 — conversion system.

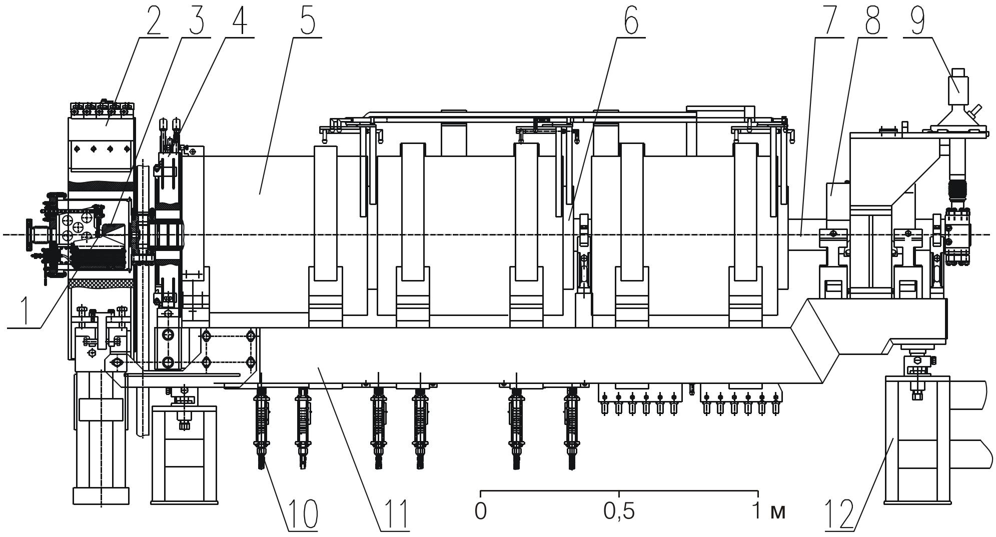

Fig. 4.22. Conversion system. 1 —conversion target, 2 —coil of the convertor, 3 —matching device, 4 — matching coil, 5 — outer coil of the solenoid, 6 — inner coil of the solenoid, 7 — acceleration structure, 8 — quadrupole lens, 9 — vacuum pump, 10 — cooling water meter, 11 — stand for the solenoid, 12 — support.

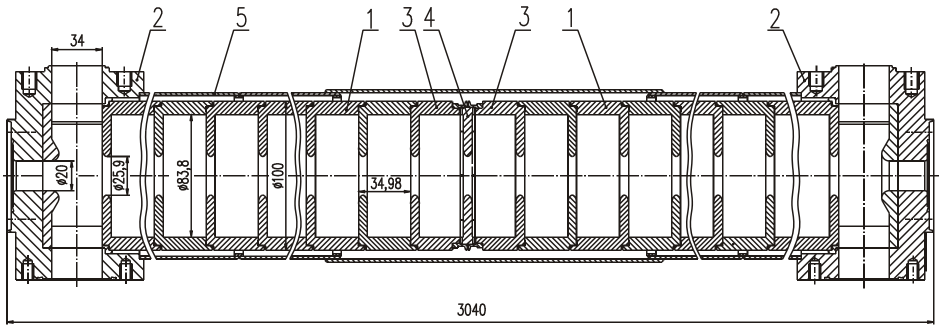

Fig. 4.23. Acceleration RF structure of the VEPP-5 injection complex. 1 — regular acceleration cell, 2 — wave-type transformer, 3 — transition (connection) acceleration cell, 4 — connecting diaphragm, 5 — water jacket.

Apart from the linear accelerators, the injection system includes a cyclic particle storage ring. After the linac, the electron or positron beams are injected into the storage ring, where they are moving along a closed trajectory in a magnetic field. After a certain number of turns, next portion of particles from the linear accelerator is added to the circulating bunch. When a required number of particles are collected, the beam is extracted to consumers. Since the coefficient of positron yield is small, most time the storage ring has to work with these particles. Electrons can also be injected into the storage ring, and they will move in the opposite direction (see Fig. 4.20). The design of the storage ring does not provide simultaneous accumulation of both types of particles moving in opposite directions.

Particles in the storage ring execute betatron oscillations relative to the equilibrium orbit, which consists of circular arcs in the bending magnets and linear segments in the straight sections between them. The straight sections of the orbit comprise quadrupole lenses that ensure sustainability of the betatron oscillations. Moving in the field of the bending magnets of the storage ring, a charged particle is emitting the so-called synchrotron radiation, which results in a radiation reaction force directed against the vector of the particle momentum. The average energy loss of particles by radiation is compensated in the storage ring by means of the RF cavity operating at a frequency that is a multiple of the rotation frequency of the beam in the equilibrium orbit. The electric field in the cavity is directed along the equilibrium orbit, and therefore fills only the loss of the longitudinal component of momentum. As a result, after a lot of turns the radiation reaction force leads to a gradual decrease in the transverse components of the particle momentum and in the amplitude of betatron oscillations [31, p. 197, 5]. In the accompanying system moving with the average speed of the beam, the chaotic particle velocity decreases, in other words, the beam is being "cooled". The equilibrium phase-space volume of the beam is mainly determined by the quantum fluctuations of synchrotron radiation [32, p. 123, 5]. The maximum intensity of the circulating bunch is limited by the coherent instabilities arising from the interaction of electromagnetic fields of the bunch with the RF cavity, inhomogeneities of the vacuum chamber, the inlet and outlet devices, etc. [33, p. 231].

The time of radiative damping of the transverse components of the particle momentum in the storage ring can be estimated as [5]

$$\tau \sim \frac{m^4 c^7}{e^4} \cdot \frac{1}{EB^2}, \qquad (4.4)$$

where E is the particle energy, B is the magnetic field value in the bending magnets of the storage ring, m is the electron mass, e is the electron charge, c is the light speed. A more exact formula must allow for the degree of orbit filling by the bending magnetic field. For the storage/cooler ring of the VEPP-5 injection complex, the time of radiation damping is approximately 20 ms, which corresponds to $2\cdot10^5$ turns of the beam.

Reduction in the phase-space volume of the beam under the influence of synchrotron radiation is crucial for the accumulation of particles. A new portion of particles from the linear accelerator is added to the circulating beam by a pulsed electric field, the action time of which is less than the orbital period of the beam in the storage ring. The radiation losses being negligible for such a short period of time, the Liouville theorem can be applied to the process of injection of particles into the storage ring [39, p. 188, 1]. According to this theorem, the phase-space volume occupied by the particles must remain the same after the merging of the two beams. Consequently, if new portions of particles are injected into the same circulating bunch with time intervals shorter than the time of radiation damping, the phase-space volume of the beam in the storage ring and the amplitude of betatron oscillations will grow until the particle start leaving the beam, falling on the walls of the vacuum chamber of the storage ring. Since the aperture of the vacuum chamber is limited by the pole gaps of the magnetic elements of the storage ring, high beam intensity can be achieved only through radiative damping, when new portions of particles are added to the vacated areas of the phase space. Thus, the productivity of the injection complex is inversely proportional to the time of radiation damping.

The considerations of minimizing the time of radiation damping apart, parameters of experiments on high energy physics also influence the choice of the working energy and magnetic structure of the storage ring. For example, the working energy of the storage/cooler of the VEPP-5 injection complex is chosen equal to 510 MeV for using the beams let out of the ring without additional acceleration for the production of φ-mesons with a mass of 1019 MeV/s^2.

Cooling the beams before their injection into the main circular accelerator that executes collisions between electrons and positrons (collider) is often applied for several reasons. Accumulation and cooling of the particles directly in the collider is in principle possible since the time of beam accumulation and cooling is much smaller than the time of beam life in the cyclic accelerator. However, injecting a beam of a large phase-space volume requires a correspondingly large aperture of the vacuum chamber of the accelerator and, therefore, it is often advantageous to use a relatively small preliminary storage/cooler ring, which allows reducing the aperture of the vacuum chamber in the subsequent electron-optical system, and, consequently, the size and cost of the magnetic elements. Besides, the loss of electrons and positrons on the walls of the vacuum chamber of the collider is a source of background events in the detector. A sharp increase in the beam size at the moment of injection leads to a corresponding increase in the level of this background, which is undesirable because it can result in failure of the sensitive recording equipment of the detector.

4.3.3. Positron source of the VEPP-5 injection complex

4.3.3.1. Electron linear accelerator

Acceleration of electrons and positrons is carried out in waveguide structures on a traveling wave (Fig. 4.23). The structure is based on the disk-loaded constant-impedance structure, through which the electromagnetic wave with a phase velocity equal to velocity of light in vacuum is passed, [30, p. 26; 35, p. 8; 34, p. 8]. The representative value of the longitudinal component of electric field in the accelerating structure is ~ 10 MV/m. Already on the first ten centimeters of the way, electrons or positrons, gaining the energy in the field of such magnitude, obtain the velocity close enough to the velocity of light and, further, move synchronously with a traveling wave.

High-power klystron UHF amplifiers of a decimeter range are used to create high tension electric fields in accelerating structures. At the VEPP-5 injection complex, the majority of structures provide an average rate of acceleration equal to 18 MeV/m. Two structures, which are accelerating the particles with low initial energies (one structure is located after the electron source, the second — after the conversion target), are supplied with a higher UHF-power, therefore, the average rate of acceleration in these structures is 25 MeV/m.

The parameters of accelerating structure require the electron source capable of producing the electron beams suitable for capture in accelerating phase of wave: the required beam energy is ~ 100 keV, the length ~ 1 cm. There are two approaches to creation of electron sources for accelerators on a traveling wave: it is possible to gain the required electron bunch via short-laser-pulse irradiation of the photocathode with the extraction electric field applied to it [30, p. 419]; or via compression in the longitudinal direction of a longer beam gained in the source on the basis of the thermo-emission cathode. The thermo-emission electron source with the subsequent time-of-flight bunching system is used at the injection complex.

Basic elements of the bunching system are RF-cavities and free sections. At passing through the cavity, particles gain different energy depending on its longitudinal position in the bunch. The phase of injection is chosen to provide the deceleration of the head particles and acceleration of the rear ones – in this case the bunch is compressed in the longitudinal direction in the free section. At the longitudinal compression, the electron bunch starts to extend in the transverse direction due to its own charge. To suppress this effect, solenoidal focusing is used at beam bunching and the movement in the first accelerating section.

To decrease the total length of the installation, electron and positron accelerators are located in parallel to each other, and the particles in them move in opposite directions (see Fig. 4.21). Before the conversion target, the electron beam is turned in magnetic field by 180˚. The isochronic scheme of achromatic turn, where, in the first order, beam energy spread does not lead to increase in its transverse and longitudinal size, is used. The elongation of electron and, hence, positron beam is undesirable, as it results in the increase of energy spread in the accelerated positron beam that complicates its injection into the cooling storage ring.

To the present time, the electron linear accelerator of the VEPP-5 injection complex is created and successfully tested at the designed parameters at 270-MeV energy (Fig. 4.21) as the conversion system (Fig. 4.22).

4.3.3.2. Conversion target

To manufacture fixed conversion targets, refractory heavy metals - tantalum, tungsten and rhenium, 73rd, 74th and 75th numbers in periodic table, respectively, are usually used. These metals possess a large nuclear charge and, hence, correspond to low critical energy $E_c \approx 10$ MeV. Besides, the given metals and also their alloys possess high mechanical strength and high fusion temperature - this is important as the conversion target should withstand repeated hits of an intensive electron beam. As a result of sharp thermal expansion of a material under the influence of an electron beam, the shock wave, which can have the intensity sufficient for target destruction is formed in a conversion target. It is experimentally determined that metal targets on the basis of tungsten-rhenium alloy are capable of a long-term withstanding the hitting of an electron beam with the energy density (per target unit area) of up to $2 \cdot 10^{12}$ GeV/mm^2 [12].

At the VEPP-5 injection complex, the electron beam focused on 1-mm area corresponds to the energy density of 0,27 GeV $\cdot\ 2 \cdot 10^{10} \approx 5 \cdot 10^9$ GeV/mm^2. Thus, in our case, the electron beam intensity is definitely less than the maximum permissible one. The average power produced in the target is also insignificant: at the electron beam pulse frequency equal to 50 Hz, it is necessary to remove approximately 30 W of heat power from a target [36].

At next-generation electron-positron colliders, such as the international linear collider ILC being now under design, the positron source productivity is required to be higher by several orders. In this case the average heat power produced in the target results in the necessity to use a rotating wheel or a stream of liquid metal as a conversion target.

At the VEPP-5 injection complex, the target material is chosen to be tantalum (radiation length $X_0 \approx 4$ mm). The cone-shape tantalum target with the minimum diameter of 2,5 mm and the length of 12 mm is fixed in the holder, which can move in the longitudinal direction by ± 2 mm from the position shown in Fig. 4.25 by means of a tie-rod. The target has also a special slot, through which the electron beam can be injected into the positron accelerator. In this case, before the target, the beam is parallel-shifted by 2 mm downwards with the help of two magnets (Fig.4.24).

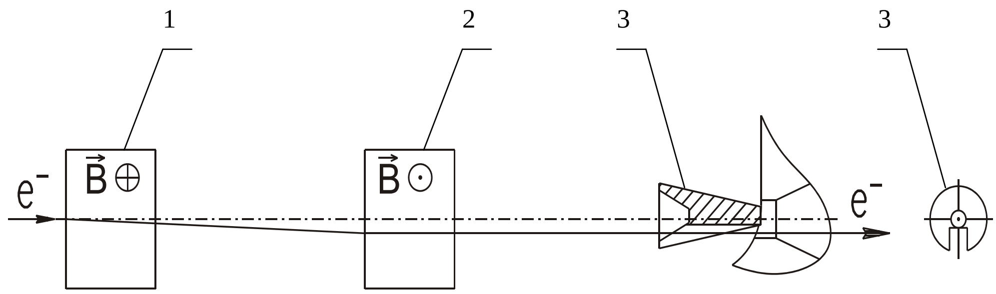

Fig. 4.24. System of parallel shift of electron beam. 1, 2 — magnets, 3 — conversion target

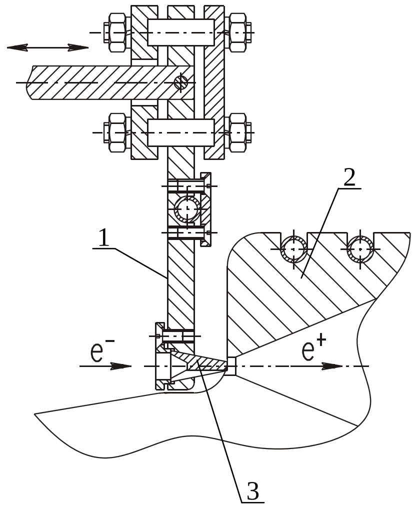

Fig. 4.25. The design of the target holder. 1 — movable target holder, 2 — pulsed magnetic lens (the flux concentrator), 3 — conversion target

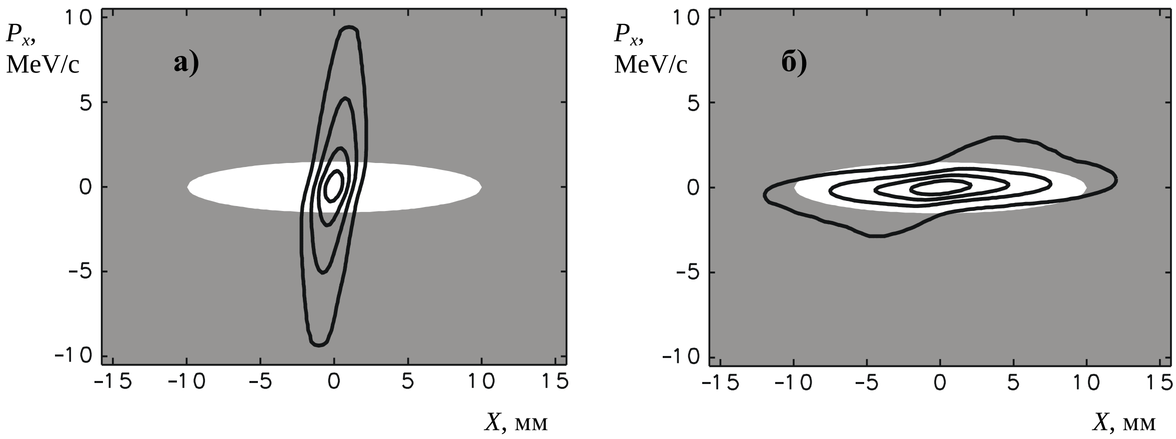

Fig. 4.26. Positron beam phase portraits represented by lines of constant density: a) after the conversion target, b) after the matching device. Grey color shows the area of P_x–X plane inaccessible for acceleration. The images are obtained by modeling the passage of positrons through axially-symmetrical magnetic field, an approximating field of the matching device of the injection complex:

$$B(z, r=0) = \frac{B_t}{1+gz}, \text{ где } g = \frac{1}{L}\left(\frac{B_t}{B_w} - 1\right), \; B_t = 10 \text{ T}, \; B_w = 0{,}5 \text{ T}, \; L = 8 \text{ см}.$$

4.3.3.3. Solenoidal focusing of positrons

The pulse transverse component of the major part of positrons, which are coming out a target, does not exceed 15 MeV/c (Fig. 4.27).

The RF-structure changes the transverse pulse of accelerated particles slightly; therefore positron trajectory inside the structure placed in the solenoid in the transverse plane will be a Larmor circle. Magnetic field of ≈ 10 T is necessary to provide fitting of Larmor orbit of the positron produced near the axis with transverse pulse of 15 MeV/c into the accelerating section with the aperture radius of 1 cm. The generation of such fields in a sufficient enough volume is possible via the superconducting magnets, the usage of which in conversion system is complicated due to a strong radiation background. The constant solenoidal field generated by the magnets with water-cooled windings is limited by the value ≈ 0,5 T. Maximal transverse pulse of positrons in such field at the chamber aperture diameter of 2 cm is equal to 1,5 MeV/c.

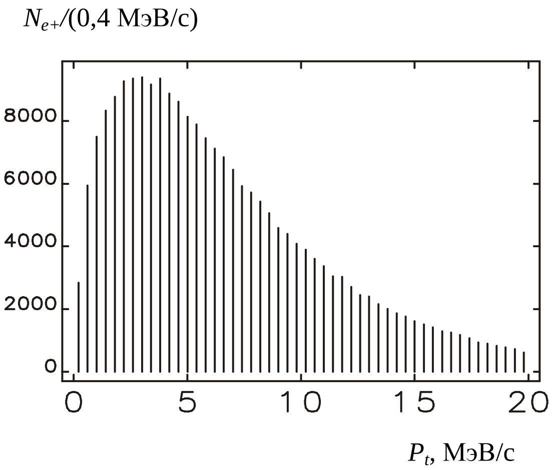

Fig. 4.27. Distribution of the transverse component of pulse of the positrons, which were produced in the conversion target**.** The spectrum is obtained by means of GEANT code [16] (quantity of the electrons hitting the target — $2\cdot10^5$, electron energy — 280 MeV, length of a tantalum target — 12 mm). The total number of the positrons extracted from the target — $2.4\cdot10^5$.

As the size of an electromagnetic shower at the target exit is usually several times less than the diameter of accelerating section aperture, there is a possibility in principle to reduce angular spread of positrons through expansion of a beam up to the diameter of accelerating section aperture via using magnetic focusing in accordance with Liouville theorem [**Error! Reference source not found.**, p. 188; 1]. The magnetic lens performing the described transformation of phase volume, i.e. focusing positrons before accelerating structure is called the matching device.

The principle of operation of the matching device is illustrated in Fig. 4.26, where phase portraits of the positron beam before the matching device and after it are represented on the accelerating structure acceptance background. By the acceptance in Fig. 4.26 we mean the projection of phase volume accessible for particle acceleration in plane P_x—X. I.e., if the particle gets to this area, it still should meet some conditions for other coordinates to be captured in the accelerating structure, but if the particle does not get inside the white ellipse — then it is surely lost on the walls of accelerating structure.

There are three main types of matching devices: the quarter-wave transformer, the magnetic flux concentrator and a plasma or lithium lens [1]. In all these devices, the pulsed magnetic field of a large magnitude is used. In a plasma lens, particles are focused by the azimuthal magnetic field appearing in the medium through which the electric current runs in parallel to a beam axis. The quarter-wave transformer is a short pulsed solenoid. The conversion target is placed at the beginning of this solenoid and its length and a magnetic field are chosen so that the transverse pulse of positrons could be compensated by the hit, which the particles gain at the solenoid exit. The basic drawback of both - the lenses with an azimuthal magnetic field and the quarter-wave transformer - is selectivity of these devices on particle energy. The quarter-wave transformer and the plasma lens focus positrons well only in a narrow part of the spectrum near the maximum.

In the matching device based on the magnetic flux concentrator, focusing of particles is used in a decaying magnetic field. The positron beam in this device extends in the magnetic field, which decays from the maximum value near the conversion target to the minimum one in the accelerating structure. The advantage of the given device is in a lesser dependence of its focusing properties on the energy of positrons. At the VEPP-5 injection complex, this type of the matching device is used; its general layout is represented in Fig. 4.28. Calculation and optimization of parameters of the concentrator were carried out by means of numerical simulation [38, 37]. In this case, optimization key parameters are the length and the maximum magnetic field in the device.

For the first time the magnetic flux concentrator was applied for gathering of positrons at Stanford linear accelerator (SLC) [6]. At first implementations of this device its length was 60 ÷ 80 cm and the maximum field - about 3 T [10, 11]. The adiabatic condition is satisfied at positron movement in such field: magnetic field change on a step of Larmor spiral is much less than the magnitude of a field. Thus, the device was called an adiabatic matching device.

Later, shorter concentrators of flux were used to focus the positrons as the effect of beam elongation due to the difference of lengths of positrons trajectories is manifested in them more slightly. Here, though the adiabatic condition for the majority of positrons is already not fulfilled, the matching device of this type is often traditionally called adiabatic or quasi-adiabatic.

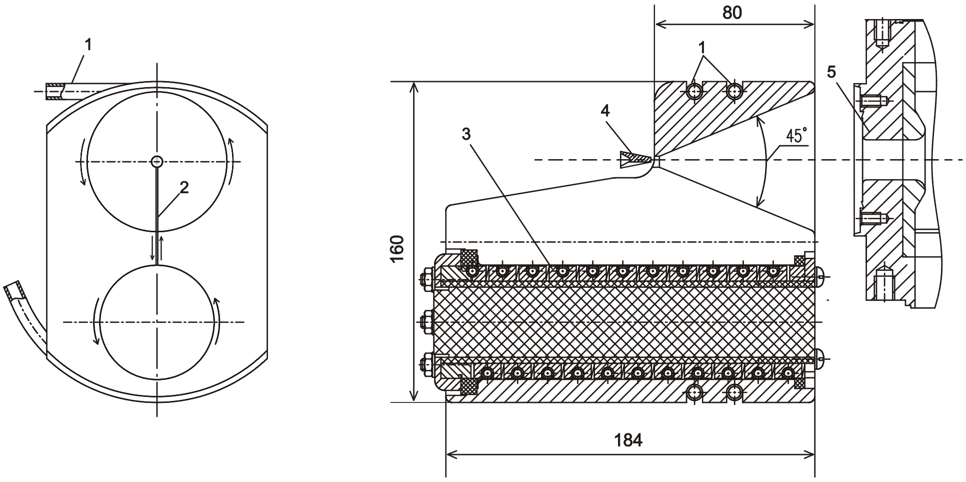

Fig. 4.28. The layout of the magnetic flux concentrator used in the positron source of the VEPP-5 injection complex. Arrows mark surface currents. 1 — water-cooling tubes; 2 — a slot between a conic cavity and a cavity of a primary winding (slot width — 0,2 mm; in the drawing the width of a slot is represented in inexact scale, since otherwise both edges of a cut merge); 3 — the pulsed coil (a primary winding); 4 — a conversion target, 5 — the beginning of the accelerating structure

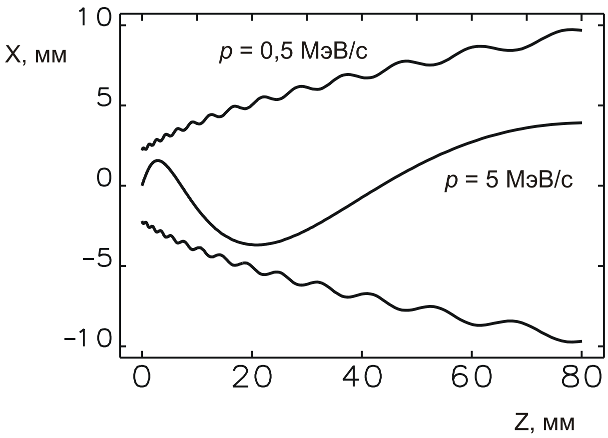

Fig. 4.29. The trajectories of positrons in a decaying field of the magnetic flux concentrator. The magnetic field decays from 10 T at Z = 0 down to 0,5 T at Z = 80 mm under the law

$$B(z, r=0) = \frac{B_t}{1+gz}, \text{ where } g = \frac{1}{L}\left(\frac{B_t}{B_w} - 1\right), \; B_t = 10 \text{ T}, B_w = 0{,}5 \text{ T}, L = 8 \text{ cm}$$

Fig. 4.28 represents the concentrator of a magnetic flux used in the positron source of the VEPP-5 injection complex. The device is the transformer, whose primary winding is the pulsed solenoid, and secondary one — the massive copper case with two cut-out cavities. As pulse duration is 20 microseconds, the current runs in a thin skin-layer of conductors (~ 0,5 mm). The

magnetic flux, created by a primary winding, is closed on the upper cavity where the required longitudinal profile of magnetic field can be obtained due to the conic geometry.
Fig. 4.29 shows characteristic trajectories of positrons in a magnetic field approximating the decaying field of the magnetic flux concentrator used at the VEPP-5 injection complex. Positrons with the energy of few MeV forming the major part of spectrum make only 1—2 turns in this field.

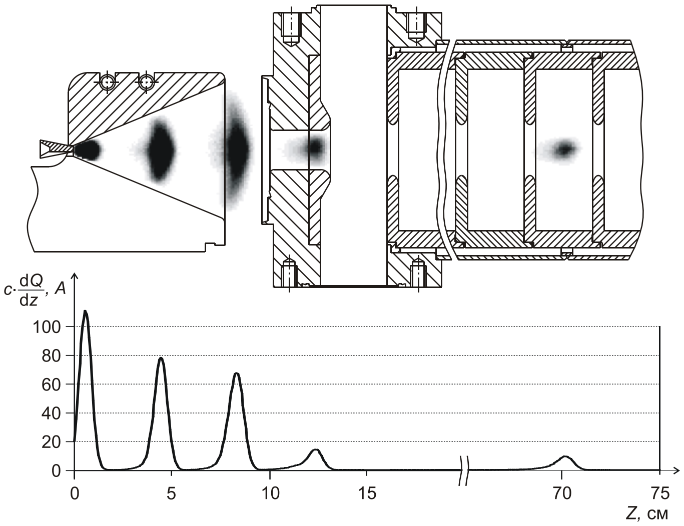

Fig. 4.30. Portraits of the positron beam at different moments of time (numerical simulation)

At creation of the magnetic flux concentrator, three basic problems related to mechanics, energy properties and optics of this pulsed magnet should be solved. Mechanics problem: the effect of electro-dynamic forces in magnet elements, first of all, in its conductive parts. The problem of mechanical fixing of winding turns becomes challenging due to impossibility of using organic insulation at intensive fluxes of ionizing radiation. Here, only ceramic insulation can be used, and only for those winding elements, which are in a weaker field and under the condition of guaranteed absence of vibrations or at the restriction of vibrations to the admissible value that excludes deterioration of ceramics-metal pair.

Elimination of the above-mentioned loosening of mechanical structure during operation is practically impossible, as these elements are, as a rule, located in vacuum, and in intensive fluxes of ionizing radiation, therefore, they are strongly activated. This condition can exclude possibility of access to these elements even after switching-off of the radiation source.

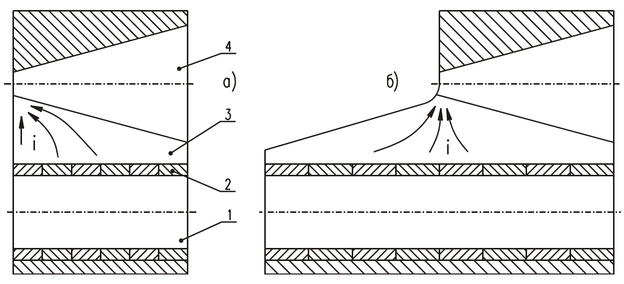

Fig. 4.31. Distribution of currents *(i)* along one of the surfaces of the slot (3) connecting the cavity of a primary winding (1) and the cavity of the flux concentrator (4). The length of a primary winding (2) is equal to the length of a conic cavity. b) The elongation of a primary winding allows the reduction of parasitic effect of the longitudinal components of currents.

Along with providing the necessary parameters of the longitudinal magnetic field, it is necessary to reduce to the minimum the axially-asymmetrical field component, which originates, first of all, due to the leak of the flux from a conic cavity of the magnet through essentially necessary slot on the edge of this cavity. Decaying profile of magnetic field (Fig. 4.31- a) inside the conic cavity, required for focusing of positrons, corresponds to strongly non-uniform distribution of current on the internal surface of a cone. This results in current deviation on the surface of a slot from the radial direction, i.e. to appearing of the currents with the component directed along a cone axis. To reduce parasitic effect of these current components, a primary winding is twice longer than a conic cavity of the concentrator (Fig. 4.31-b). Such elongation of a primary winding allows the reduction of parasitic effect of the longitudinal components of surface currents.

Main parameters of the magnetic flux concentrator are the following:

- The maximum value of magnetic field 10 T,
- Total current of the magnet conic cavity 120 kA,
- The maximum voltage of the capacitor storage 1,2 kV,
- Power consumption of the capacitor storage 90 J,
- Pulse duration of current 26 microseconds,
- Frequency of work 50 Hz,
- Average power consumption 4 kW.

4.3.3.4. Stand testing of the magnetic flux concentrator

After development and manufacturing of the pulsed magnet, its stand testing with proper pulse generator has been carried out. Magnetic measurements were performed by means of the inductive sensor supplied with the RC-integrator [7]. Fig. 4.32 represents distribution of the longitudinal and transverse magnetic field in the magnet cone.

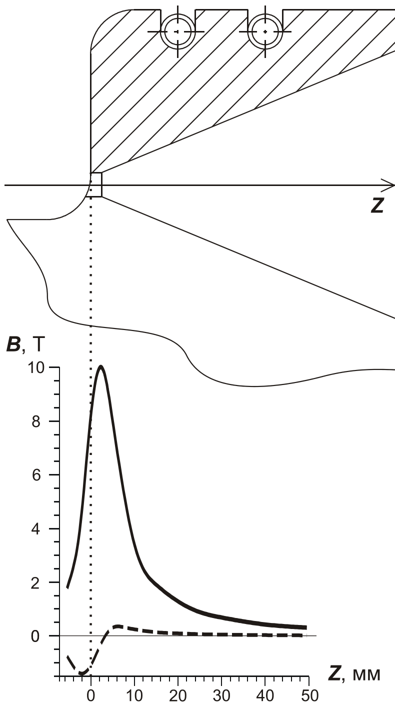

Fig. 4.32. Results of measurement of magnetic field of the concentrator. A solid line — longitudinal field, dotted — the transverse field.

The magnet has worked at the stand about 10^7 cycles without any faults or change of its parameters.

The conversion target placed in a strong pulse magnetic field, considerably warms up, however, the cooling provided by a design of the target holder ensures the heating of an end face of the target not more than 100°C. Magnetic field perturbation at an end face of such "semitransparent" (thickness of skin layer ≈ 1 mm) for pulsed magnetic field target also appeared to be insignificant. Magnitude of pulsed field decreases only by 2÷3 % at a distance of 1 mm from the target end face.

4.3.3.5. Quadrupole focusing of positrons

Quadrupole focusing is economically more favorable than solenoidal one as it does not require creation of magnetic field in the whole volume of the vacuum chamber; but the beam focused by quadrupole lenses should be monochromatic enough. Quadrupole focusing is usually used in the positron sources at beam average energy more than 100 MeV when energy spread is ≈ 20 %.

To pass to focusing by quadrupole lenses without particle losses is possible only in the case when the quadrupole channel acceptance matches the beam emittance at the solenoid exit. The acceptance of quadrupole channel can be estimated as

$$A \approx \frac{r^2}{L_q} p, \tag{4.5}$$

where r is radius of the vacuum chamber aperture, L_q — distance between the centers of quadrupoles, p — an average momentum of positrons. By acceptance we mean here the phase area in co-ordinates (x, p_x) or (y, p_y). This estimation is close to an exact value in the case when change of energy of positrons between two lenses is small in comparison with their energy at the solenoid exit.

The solenoid can be can passed through by the positrons, the transverse momentum of which is less than the value

$$P_{t,\max} = reB_w, \tag{4.6}$$

where e — positron charge, B_s — magnetic field in the solenoid. For parameters of the VEPP-5 injection complex, $P_{t,\max} \approx 1{,}5$ MeV/sec. The area of phase plane (x, p_x), accessible for acceleration of particles inside the long solenoid, is restricted by an ellipse with the area

$$A_s = \pi r P_{t,\max}. \tag{4.7}$$

The filling of this ellipse by positrons depends on parameters of the matching device. Fig. 4.33 represents the distribution of positrons on planes (x, p_x), which corresponds to the parameters of the VEPP-5 injection complex.

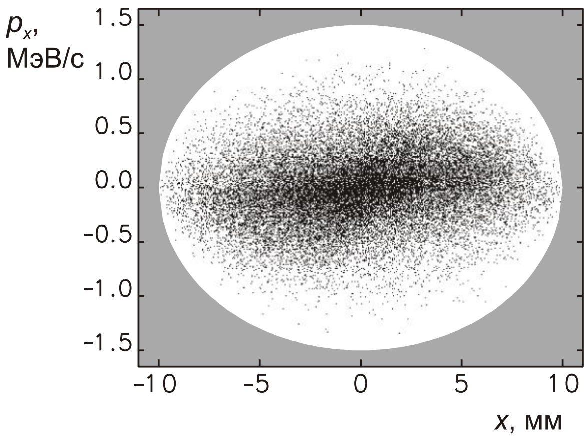

Fig. 4.33. The phase portrait of the positron beam at the end of the solenoid (numerical simulation). The solenoid acceptance is shown by a white oval.

According to Fig. 4.33, a beam at the end of the solenoid occupies the entire accessible aperture; and the distribution of particles is twice narrower than the accessible interval from–$P_{t,\max}$ to $P_{t,\max}$ on the axis of pulses (see Fig. 4.34). The similar situation with slight changes is characteristic for all matching devices and reflects the fact that the closer is the positron transverse momentum to restriction $P_{t,\max}$, the easier for this particle to hit walls of a vacuum chamber in the solenoid. From the distributions shown in Fig. 4.33 and Fig. 4.34, it follows that 90 % of positrons occupy on a phase plane the area twice smaller than the area estimated by the expression (4.7).

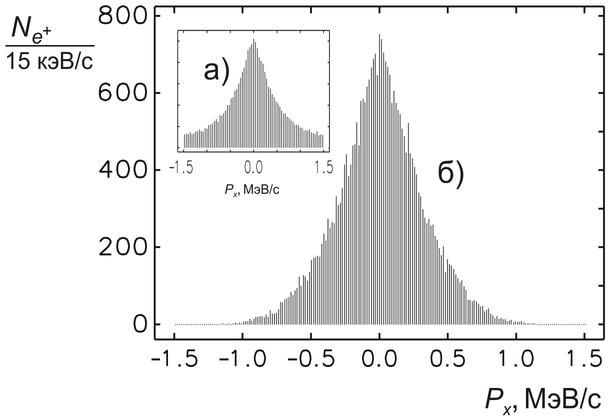

Fig. 4.34. Distribution of the number of positrons vs horizontal momentum: a) at the beginning of the solenoid b) at the end of the solenoid

Thus, the equation for energy of transition between solenoidal and quadrupole focusing, at which the loss of positrons is less than 10 %, is as follows:

$$\frac{r^2}{L_q} \approx \frac{\pi}{2} \cdot \frac{rP_{t,\max}}{E_{tr}/c}, \tag{4.8}$$

where E_{tr} is transition energy. Hence, we express E_{tr}

$$E_{tr} \approx \frac{\pi}{2} \cdot \frac{L_q}{r} \cdot cP_{t,\max} = \frac{\pi}{2} \cdot B_s L_q ec. \tag{4.9}$$

At the VEPP-5 injection complex, the distance between the lenses, which are located in the accelerating sections, L_q = 1,7 m (see Fig. 4.35); field in solenoid B_s = 0,5 T; hence, $E_{tr} \approx$ 400 MeV.

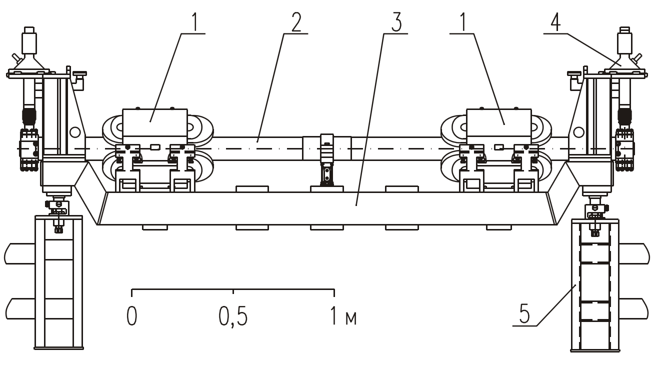

Fig. 4.35. Accelerating structure with quadrupole lenses. 1 — quadrupole lens, 2 — accelerating structure, 3 — support, 4 — vacuum pump, 5 — support stand

Currently, at the injection complex, $E_{tr} \approx 70$ MeV; this results in high losses of positrons (about 2/3 from the number of those passed through the solenoid). In the future, increase of the length of the conversion system solenoid and installation of additional quadrupole lenses to double the yield of positrons are planned.

Fig. 4.36 shows the minimum sizes of the positron beam which can be provided by quadrupole focusing in the positron accelerator of the injection complex (without restriction on the vacuum chamber aperture). As seen from Fig. 4.36, the beam transverse size becomes smaller than its initial size in the solenoid only at the end of the linear accelerator where the energy of positrons is over 400 MeV; this corresponds to the estimations performed earlier.

Fig. 4.37 shows how the number of positrons decreases with the beam movement along the accelerator due to the losses of positrons on vacuum chamber walls.

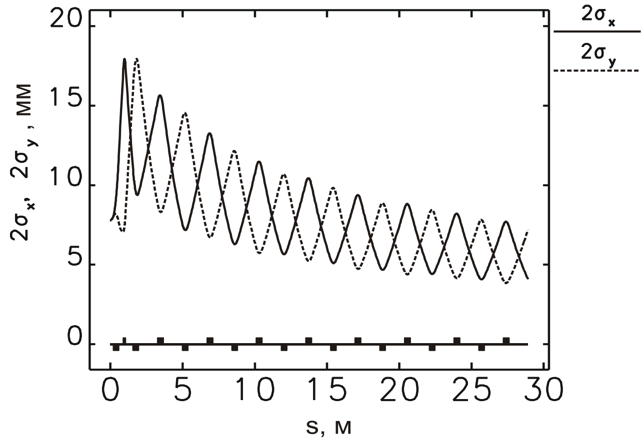

Fig. 4.36. The minimized transverse sizes of the beam in the positron accelerator of the injection complex (without taking into account restriction on the vacuum chamber aperture). Calculations are made in ELEGANT code [13]. Quadrupole lenses are shown by rectangles at the bottom of the diagram

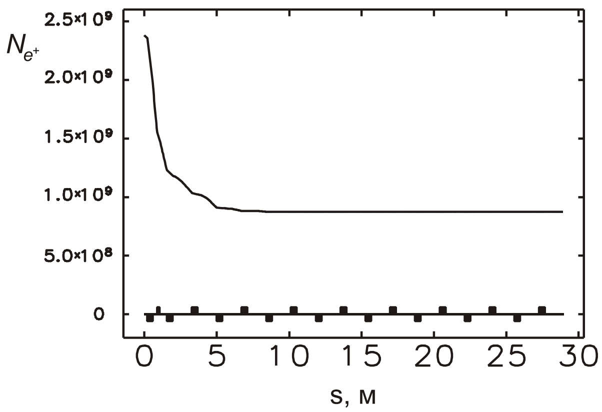

Fig. 4.37. Quantity of positrons vs the beam position along the linear accelerator of the injection complex (from the conversion system solenoid to the injection channels of the cooling storage ring). Simulation is made by ELEGANT code [13]. Quadrupole lenses are shown by rectangles at the bottom of the diagram.

4.3.3.6. Injection of the positron beam into the cooling storage ring

The characteristic feature of the cooling storage ring, as well as of many cyclic accelerators, is its rather small energy acceptance, i.e. the maximum permissible energy spread in the injected beam. For the cooling storage ring of the VEPP-5 injection complex, the maximum deviation of particle energy from the equilibrium one is $\Delta E/E_0 = \pm 0{,}012$.

The energy spread of the positron beam at the end of the linear accelerator is defined by the ratio of beam length and wave length of the accelerating RF-field. Usually this energy spread is more than maximum permissible spread for the storage ring, therefore, an additional matching device — debuncher-monochromator is used at many installations before injection of positrons into the storage ring. This device provides a turn of the positron beam in plane E — s (energy — longitudinal coordinate), thus, reducing the energy spread via increasing the beam longitudinal size.

Fig. 4.38 represents the scheme of debuncher-monochromator operation at the VEPP-5 injection complex.

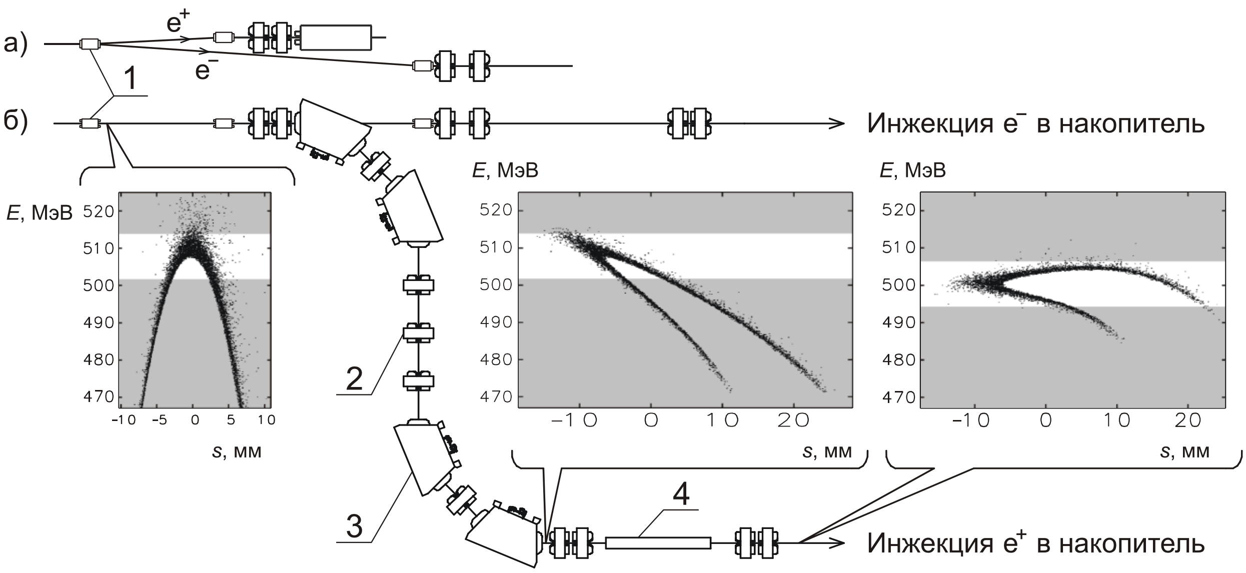

Fig. 4.38. a) Scheme of separation of positrons and electrons before injection into the cooling storage ring (side view). B) Scheme of positron beam debuncher-monochromator (top view). 1 — dipole magnet separating electrons and positrons in a vertical plane; 2 —quadrupole lens; 3 — bending magnet; 4 — accelerating structure. The inserts show the portraits of the positron beam on plane E — s (energy — longitudinal coordinate) in various points of the channel. White strip denotes the energy acceptance of the cooling storage ring

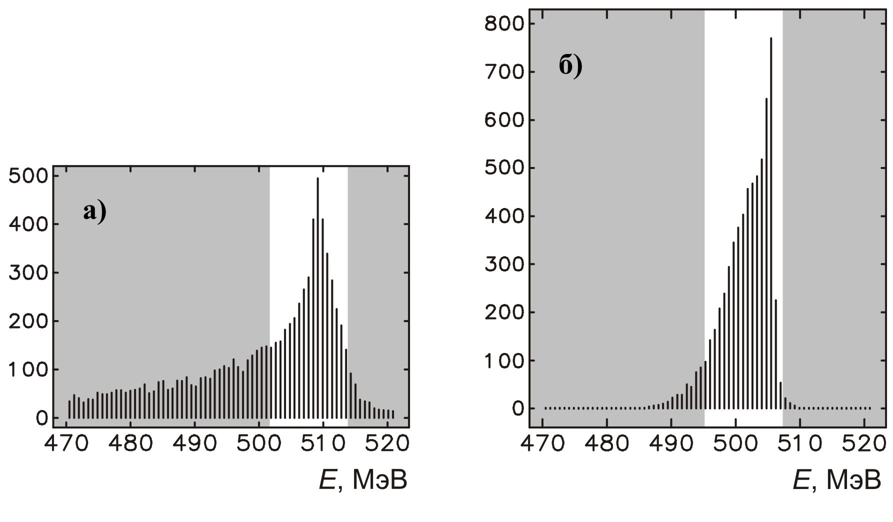

Fig. 4.39. Estimated spectrum of the positron beam: a) at the end of the linear accelerator, b) after the debuncher-monochromator. White strip denotes energy acceptance of the cooling storage ring.

It is supposed to direct positrons to the storage ring through the channel consisting of four 45-degree bending magnets. The particles of a higher energy move in the field of bending magnets along the trajectory with a larger radius and get to the tail-end of a beam; thus, the particles with a lower energy get to the head-part of the beam. The energy spread in the beam, arranged in such manner, can be partially reduced via passing a beam through the accelerating structure close to a zero phase of electric field. Fig.4.39 represents estimated spectra of the positron beam before and after the debuncher-monochromator.

The calculations show that usage of debuncher-monochromator at the VEPP-5 injection complex will allow increasing the number of the positrons captured into the storage ring by 1,5 times.

4.3.3.7. Results of the experiments, measurement of the yield factor of Y positrons

To determine yield factor of *Y* positrons, measurements of all three values of the formula (4.3) have been performed: E, N_- and N_+.

Measurement of electron beam charge before the conversion target was made via using the Faraday cup. The Faraday cup is made of tungsten, its length is 70 mm, width and height are 20 mm. Simulation in GEANT code [16] shows that charge absorption in the cylinder is 94 % (the cylinder of total absorption could not be used because of a free-space deficiency). To prevent the current of secondary electron emission from a cylinder surface, a 300V-voltage, being positive relative to the vacuum chamber, is applied to the cylinder. Electron beam charge was calculated using the oscillogram of the current coming from the Faraday cup.

Electron energy was measured after the bending magnet using the beam image on a sliding luminescent screen (see Fig. 4.40).

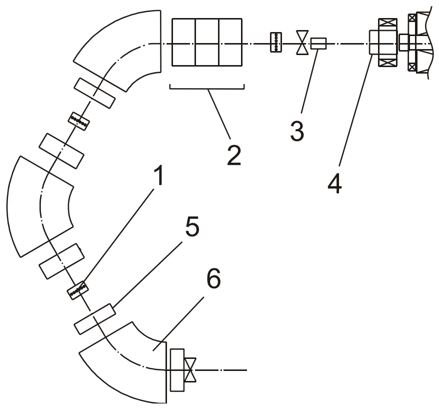

Fig. 4.40. Isochronous beam turn before the conversion system. 1 — luminophor flag, 2 — focusing triplet, 3 — Faraday cup, 4 — conversion system, 5 — lens, 6 — bending magnet. Quadrupole lens 5 is switched off during measurement of electron beam energy.

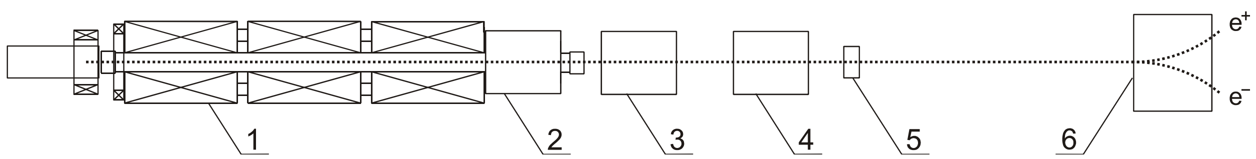

Fig. 4.41. The installation used for measurement of positron yield factor. 1 — conversion system solenoid, 2, 3, 4 — quadrupole lenses, 5 — beam position corrector, 6 — magnet-separator

To measure the quantity of the positrons produced by the conversion system, it is necessary to separate positrons from the electrons, which are accelerated in the adjacent phases of the RF-structure traveling wave. The rectangular dipole magnet was used for this purpose (magnet-separator in Fig. 4.41).

Three quadrupole lenses are placed between the conversion system solenoid and the magnet-separator for beam focusing. The results of calculation of positron losses in the vacuum channel from the solenoid to the end of the magnet-separator are shown in Fig. 4.42.

The simulation showed that, at optimum values of magnetic field gradient in lenses, not more than 80 % of positrons from the number of positrons accelerated in completely assembled positron accelerator can pass through the channel used for measurements (Fig. 4.43). Thus, measurement of the positron beam charge after the magnet-separator should not give unreasonably exaggerated estimation of the efficiency of the whole injection complex.

s

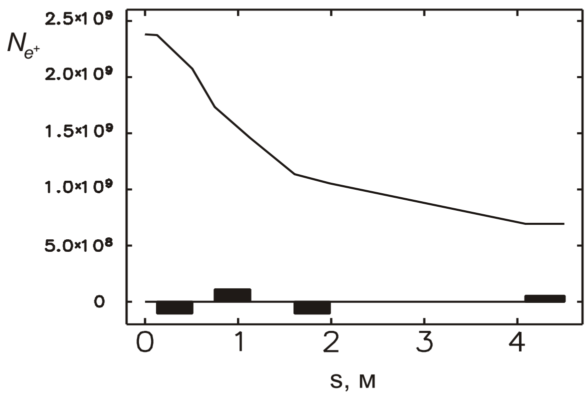

Fig. 4.42. Quantity of positrons vs beam position along the vacuum channel of the experimental installation. Three quadrupole lenses and a magnet-separator are shown by rectangles at the bottom of the diagram. Simulation was made by ELEGANT code [13].

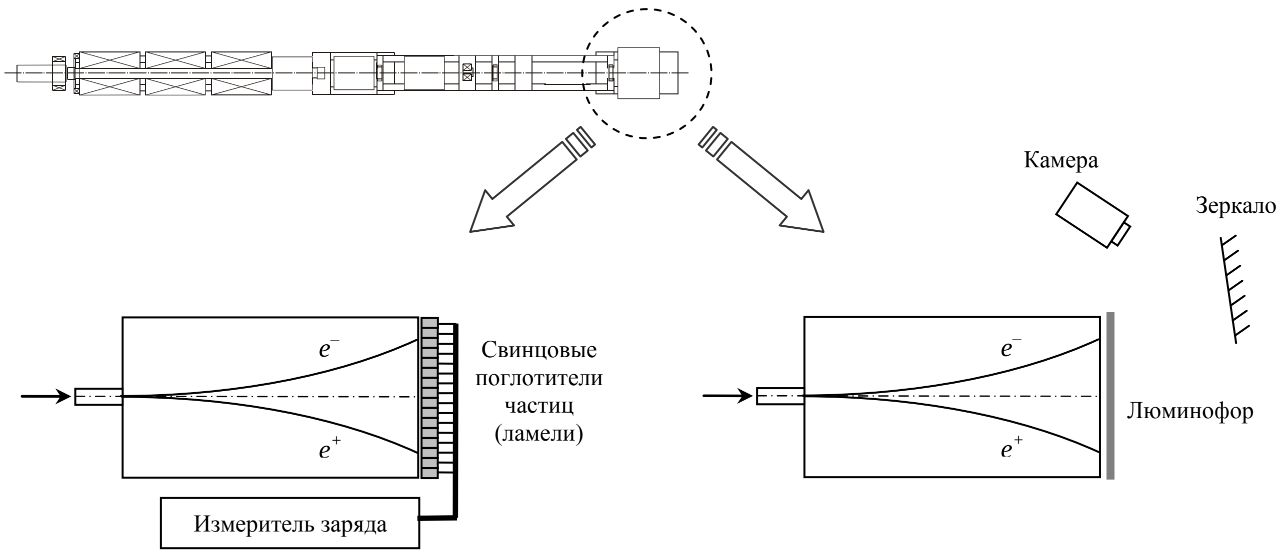

Fig. 4.43. Systems of particle registration.

To measure the charge and average energy of the positron beam, the sectioned receiver consisting of 16 lead sections (lamellas) was installed after the dipole magnet-separator. Section width is 10 mm, length is 50 mm. Sections are isolated from each other by a glass-fiber laminate. The incident beam is completely absorbed in the receiver. Measurement of the charge got on a lamella is made by the device consisting of 32 charge-sensitive amplifiers [**Error! Reference source not found.**, p. 270], commutated on ADC in turn. Measurement was made from each lamella separately, and then the bunch charge was computed by summation. Fig. 4.44 shows the dependence of the number of positrons on the field maximum in the matching device at different energies of the electron beam hitting the target.

At 265-MeV electron energy, the quantity of the positrons registered after the magnet-separator is $5 \cdot 10^8$. The number of electrons before the target measured by means of the Faraday cup is $1{,}8 \cdot 10^{10}$. Thus, the conversion ratio (4.3) for the given system is $Y \approx 0{,}1$ GeV^{-1}.
To measure spatial particle distribution in a beam, the luminescent screen has been installed after the magnet-separator instead of lead absorbers. Light flash on luminescent screen induced by beam hit was registered by means of the CCD-camera synchronized with the accelerator operation. Fig. 4.45 represents the image registered by the camera.

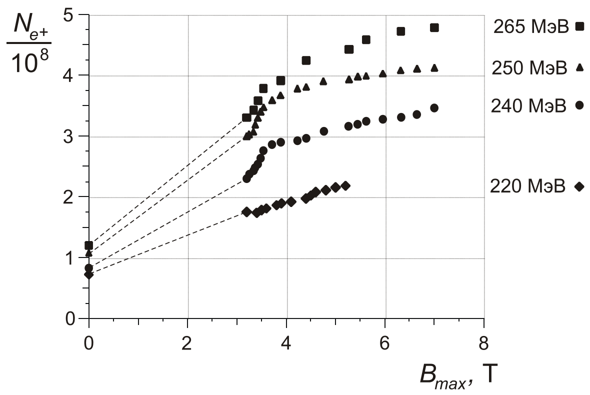

Fig. 4.44. Number of the accelerated positrons vs the concentrator magnetic field value for different energies of electron beam.

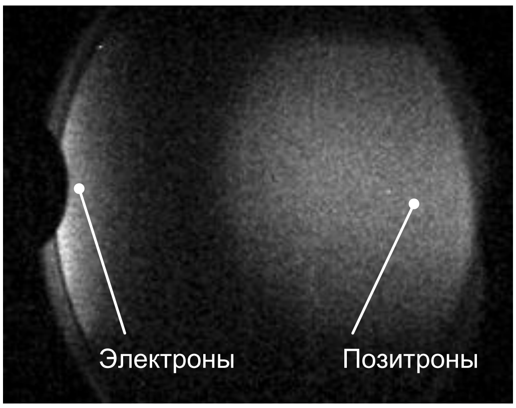

Fig. 4.45. The image on the luminescent screen.

4.3.3. Conclusion

Tests of conversion system of the VEPP-5 injection complex have shown that the given installation is capable of producing up to $5 \cdot 10^8$ positrons per a pulse. Losses of positrons at injection into the cooling storage ring according to the estimations should be approximately a half of this number, therefore, the possible total yield of the injection complex at operation frequency of linear accelerators of 50 Hz can be expected to be up to 10^{10} positrons per second.

The main advantage of the VEPP-5 injection complex over analogous installations, as seen from Table 1, is the matching device of the improved design, which provided the optimal magnetic field value for positron focusing, without violating the axial symmetry of this field. The disadvantages are: small length of the solenoid providing focusing of positrons at the beginning of the accelerator and a small number of quadrupole lenses, these results in unavoidable losses of positrons at beam passing through transition area between solenoidal and quadrupole focusing. One more constructive deficiency of the positron system is absence of the magnetic system separating positrons from electrons at the beginning of the accelerator (after the solenoid). The electron bunch, being behind the positrons by half-length of RF wave, will fly through the whole accelerator till the cooling storage ring complicating the adjustment of the installation. The magnets for separating electrons were not provided at the injection complex to save the space for the linear accelerator of positrons.

Future increase of the complex productivity is possible in several directions: via improvement of magnetic focusing of positrons, increase in intensity and energy of a primary electron beam. The elongation of the conversion system solenoid and also installation of additional quadrupole lenses at accelerating sections can exclude the losses of positrons after the solenoid (Fig. 4.37) and double or triple the output of positrons. Usage of an updated electron source can provide the increase of the number of electrons (approximately by 3 times, up to $6 \cdot 10^{10}$) in a beam hitting the target (further increase in electron beam intensity is restricted by the effects of RF-field distortion under the influence of the electromagnetic fields radiated by a beam into the accelerating structure). Besides, there is a possibility for a 1,5-time increase of the electron beam energy via installation of additional accelerating structures. Thus, 10^{11} positrons per second, is, probably, the ultimate productivity, which can be provided by the VEPP-5 injection complex.

4.4. The linear accelerator

The linear accelerator (LA) of $c\tau$-factory is intended to provide effective injection of electrons and positrons into collider at the energy of performing the experiments up to maximum E = 2.5 GeV. The accelerating waveguide structures on a traveling wave, which are already used at BINP at the VEPP-5 injection complex, are planned to be applied at $c\tau$-factory LA.

Vertical and a horizontal acceptance of $c\tau$-factory is determined by geometrical aperture of the lenses of final focus and is $A_x = 23\sigma_x$ and $A_z = 60\sigma_z$, or, in absolute values A_X = 4250 nm-rad and A_Z = 180 nm-rad.

Positron beam emittances at the exit of the cooling storage ring at energy E = 510 MeV are equal to ε_x = 23 nm-rad, ε_z = 5 nm-rad. After acceleration in the linac, the emittances will decrease adiabatically and will be: ε_x = 11 nanometers-rad, ε_z = 2.5 nm-rad at $E_{inj} = 1\,\text{GeV}$ and ε_x = 4.6 nanometers-rad, ε_x = 1 nm-rad at $E_{inj} = 2.5\,\text{GeV}$.

The electron beam, which is accelerated from a photo-gun to a full energy in linac, will have: ε_x = z ε= 10 nm-rad at $E_{inj} = 1\,\text{GeV}$, and ε_x = z ε= 5 nm-rad at $E_{inj} = 2.5\,\text{GeV}$ with power spread $\sigma_E \le 1 \cdot 10^{-3}$.

The cooling storage ring emits positrons with power spread $\sigma_{E0} = 5 \cdot 10^{-4}$. The length of a bunch at the storage ring exit is σ_{s0} = 0.3 cm. After additional acceleration in the linac with the wave length λ = 10 cm, beam energy spread, due to the phase extent of a bunch, will increase by an order. Efficiency of injection of such beam into the storage ring of $c\tau$-factory will not be above 60÷70%.

To decrease the energy spread of positrons after additional acceleration in the linac, a bunch of positrons, before injection to the linac, should be compressed by 2÷3 times. For this purpose, a section of the linear accelerator of 15÷20 MeV should be installed in the extraction positron channel, after 90°-turn (hall №.2). At the section exit, the energy spread in a beam will be increased by 4÷5 times, and after passing the achromatic section of descent to the tunnel, with the longitudinal dispersion function $\eta_s \approx$ 50 cm, the bunch length will decrease. After these manipulations, the energy spread at the entry of the of $c\tau$-factory storage ring will be $\sigma_E = 1 \div 2 \cdot 10^{-3}$, and the bunch length - $\sigma_s \approx 0.5$ cm (the bunch will become longer after passing the injection channel to the $c\tau$-factory where $\eta_s \approx 250$ cm).

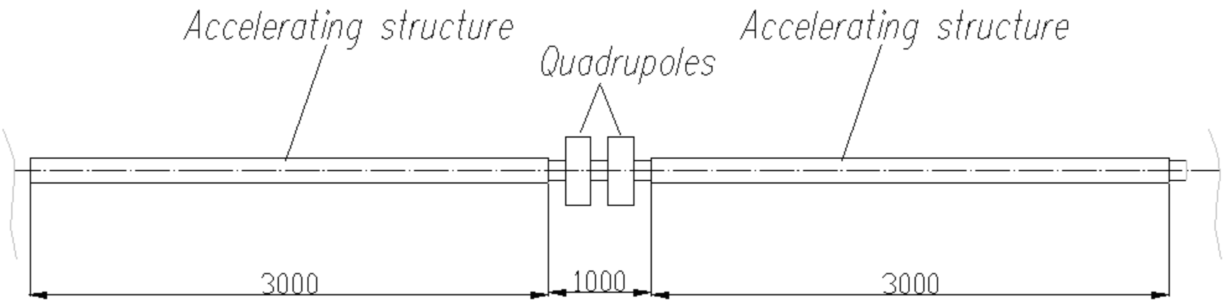

Fig. 4.46. Schematic view of the accelerator module.

Thus, the linear accelerator, which should accelerate positrons up to energy of 2 GeV and the electrons, produced by the source of polarized electrons, up to 2.5 GeV is necessary. The structures on a traveling wave are suggested to be used as the accelerating structures. They are the disk-loaded waveguide structure with constant impedance, phase shift on a cell of 2π/3 and phase velocity of the main accelerating harmonic equal to the velocity of light. Positrons get to a regular part of the accelerator, which consists of the accelerating structure and OFODO cell, therefore, are not considered separately.

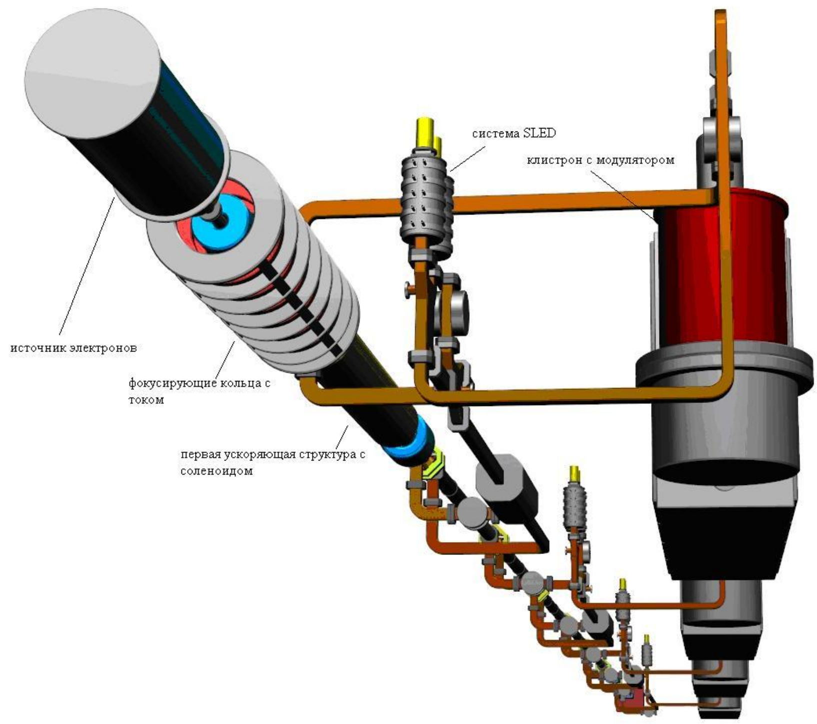

Fig. 4.47. General view of the electron accelerator.

The general scheme of the accelerator will consist of the modules (Fig. 4.46), which include one klystron with the modulator, power compression system SLED-type of SLED-type, two accelerating structures and two waveguide loads. Between the structures, it is necessary to provide the gap, in which OFODO cell, beam diagnostics system and a vacuum gate-valve should be placed. The general view of the accelerator is represented in Fig. 4.47.

After the source of polarized electrons, the beam has the energy $W \approx 100\,\text{keV}$ and duration $t_b \approx 2$ nanoseconds. To increase the quantity of accelerated particles and to decrease the energy spread in a beam, the bunching system should be placed between the electron source and the first accelerating module. The given system will consist of the subharmonic cavity and the buncher on the main frequency of the accelerator $f_0 = 2856\,\text{MHz}$.

For the longitudinal compression of electron bunch of 2-nanosecond length, a subharmonic buncher should possess the period twice larger than the beam length, i.e. 4 nanoseconds. Thus, the frequency is equal to 250 MHz. It is rational to make the cavity with the frequency below the necessary one, so that the wave half-period in it were slightly larger than the beam length, for example $f_S \approx f_0/12 = 238$ MHz. To provide the decrease of the beam longitudinal size by ~6 times before injection to the buncher at the main frequency, a free section is necessary after the cavity. The length of the section will be determined after calculation of particle dynamics, and is estimated to be up to 1.5 m.

The buncher on the main frequency can be produced as a three-cell cavity with an oscillation mode π used for a long time at the VEPP-5 pre-injector. The advantage of such cavity is in the fact, that at the exit, its bunch is already bunched and is ready for injection into the accelerator.

Also, for the electron accelerator, the focusing system placed after the electron source is very important. As Coulomb repulsion forces will increase at beam compression after the subharmonic cavity, the increase of magnetic field, in which a beam should move, is necessary. Such increase of the field can be formed by means of the rings with current, which are placed correctly. Besides, while passing the first accelerating structure, the beam should always be in solenoidal magnetic field.

4.4.1. RF system of the linear accelerator

4.4.1.1. Klystron

Klystron TH 2128 C/D, Thales-produced, is suggested to be used as RF power source. Average power of such klystron is 10 kW, this corresponds to repetition frequency of 50 Hz at 4-microsecond pulse duration. Its parameters and view are represented in Table 4.7 and Fig. 4.48, respectively.

Table 4.7. Main parameters of TH 2128 C/D Klystron

RF frequency	2856 MHz
Peak output power	45.5 MW
Average power	10 kW
RF pulse duration	4 microseconds
Gain	54 dB
Efficiency	43 %
Max. input power	200 W
Bandwidth	10 MHz
Cathode voltage	315 kV
Beam current	335 A
Cathode heating voltage	30 V
Cathode heating current	24 A

Fig. 4.48. View of the klystrons of TH 2100-series (at the left) and the modulator K2-3

Modern pulsed high-voltage power supply of the given klystron is produced by the several companies. For example, the equipment produced for such klystrons by the Swedish company “ScandiNova Systems” (http://www.sc-nova.com/) – modulators K2-1/K2-3 (Table 4.8).

Table 4.8. Parameters of the modulators of K2-series (ScandiNova Systems)

Parameter	Unit	K2-1	K2-2	K2-3
Pulse output RF power of klystron	MW	35	40	45
Average output RF power of klystron	kW	1.6	1.6	1.6
Pulse power of modulator	MW	74.3	91.5	100.5
Average power of modulator	kW	4.3	5.0	5.1
Pulse voltage	kV	270	300	314
Pulse current	A	275	305	320
Pulse repetition frequency	Hz	1-10	1-10	1-10
Pulse duration	μsec	4.5	4	3.5
Uniformity of pulse flat part	%	± 1	± 1	± 1
Pulse shape repeatability	%	± 0.2	± 0.2	± 0.2

The given modulator (Fig. 4.48) is the complete solution of providing a regular work of the klystron. It includes all necessary components for this device: the high-voltage charger, PFN, solid-state high-voltage switches, the pulsed high-voltage transformer, klystron heating power supply, control, diagnostic and interlock systems.

4.4.1.2. SLED system

The power compression SLED-type system is applied at the VEPP-5 pre-injector (Fig. 4.49). The parameters of such system are represented in Table 4.9.

Table 4.9. Main parameters of the power multiplication system

Cavity diameter, *D*	196 mm
Cavity height, *H*	346.6 mm
Operation frequency, f_0	2856 MHz
Tuning range, Δf ($\Delta f/\Delta H$)	±5 MHz (2.75 MHz /mm)
Unloaded Q-factor, Q_0	53200
Coupling coefficient with supplying waveguide, β	5.84
Time constant, τ_0	5.93 microseconds
The loaded time constant $T_C = \tau_0/(1+\beta)$	0.87 microseconds
Time of phase reversal (180^0)	3 microseconds
Klystron pulse duration	3.5 microseconds
Voltage multiplication factor K_0	2.67

Fig. 4.49 also shows a typical dependence of RF power at the exit of the power compression system on time. The values of corresponding parameters of power compression system (of SLED-type) are represented in the Table 4.9. Difference of real dependence from the ideal one is connected with finiteness of fronts of the klystron RF-pulse, a nonzero time of phase reversal and with resistance losses in the compression system.

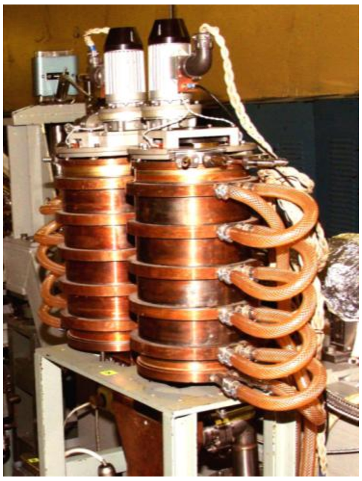

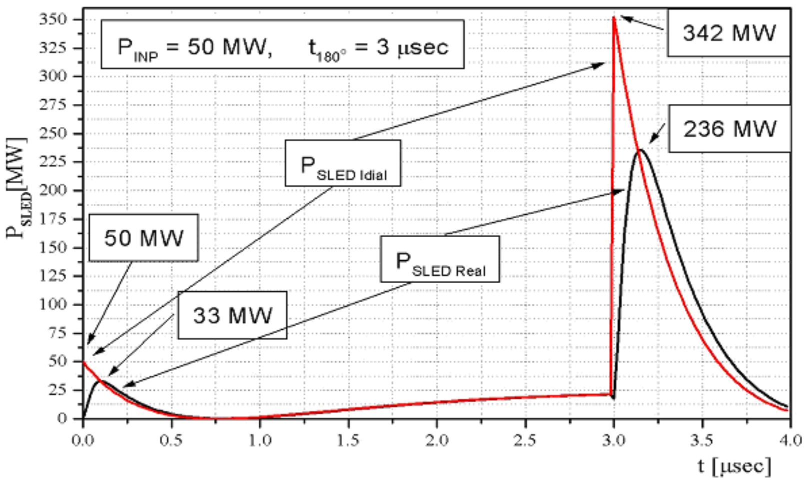

Fig. 4.49. SLED power multiplication system produced in BINP SB RAS (at the left). RF power at the SLED system exit vs time for ideal (red curve on the right) and real (black curve) cases.

4.4.1.3. Bunching system

The bunching system for the beam from the source of polarized electrons is represented as two cavities-bunchers and a free space between them.

The first cavity, which is a sub-harmonic buncher, operates with an oscillation mode E_{010} at frequency $f_S \approx f_0/12 = 238$ MHz. It should compress a beam approximately by 6 times before injection into the buncher at the main frequency of the accelerator. A free section of 1.5-m length should be provided between two cavities for beam bunching.

The second cavity is made as a three-cell cavity with oscillation mode π. Its view is represented in Fig. 4.50. Fig. 4.51 shows the electric field distribution on the cavity axis.

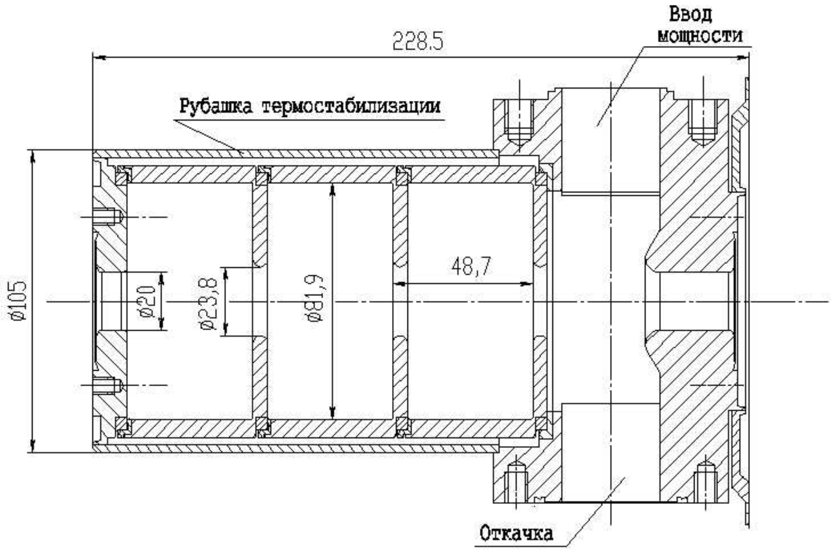

Fig. 4.50. The cavity-buncher at the main frequency of 2856 MHz

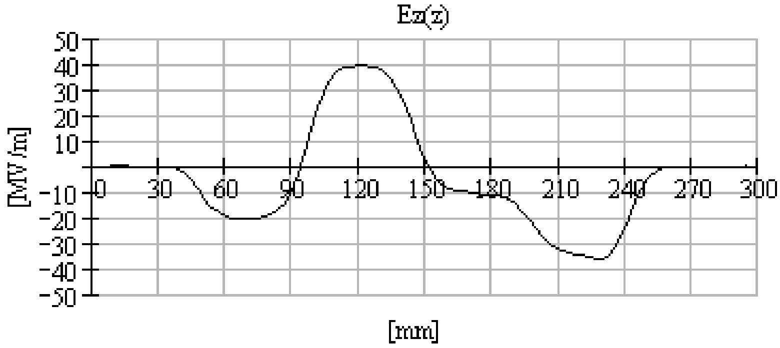

Fig. 4.51. Electric field strength on the cavity-buncher axis at the main frequency with the stored energy of 1 J

4.4.1.4. Accelerating section

The operation scenario of the linear accelerator of *S*-range on a traveling wave with the power compression system is as follows: RF power pulse, analogous to the pulse in Fig. 4.49, is divided between the necessary quantity of accelerating structures (AS), and through phase shifters comes to their inputs. Electric field strength reaches the maximum value at the very beginning of the structure, at the moment, when the maximum power after multiplication system starts passing through the AS. If this strength exceeds a certain value, then RF breakdowns originating in this case in the beginning of the structure will result in a beam loss. For our AS design the maximum strength of accelerating electric field obtained experimentally is ≤ 40 MV/m. Then, RF power is spread along the structure with a group velocity and in the time interval equal to the time of filling the structure starts to enter the matched load. This very moment is optimal for acceleration of the electron bunch.

Table 4.10. AS main parameters

Operation frequency	2855.5 MHz
Operation mode of oscillations	$2\pi/3$
Length, L	2.93 m
Unloaded Q-factor, Q_0	$1.32\cdot10^4$
Group velocity, V_{gr}	$0.021\cdot C$
Shunt impedance	51 MOm/m
AS unloaded constant, $\tau_0 = 2\cdot Q_0/\omega$	1.47 μs

AS field damping factor , $\alpha = 1/(\tau_0 \cdot V_{gr})$	0.108 1/m
Damping parameter αL	0.316
AS Filling time, $T_f = L/ V_{gr}$	0.465 μs
Period	34.98 mm
Inner diameter of the cell cavity	83.8 mm
Iris aperture diameter	25.9 mm
Iris thickness	6 mm
Overvoltage coefficient	1.7

In our case one klystron and one power compression system SLED feed two accelerating sections. Section parameters are given in the Table 4.10. Total gained energy in ideal variant without taking into account a beam from one section is 70 MeV (Fig. 4.54). As it is seen from the scheme in Fig. 4.53, field strength in the first cell of the section is close to critical 40 MV/m. Thus, the acceleration gradient of 23 MeV/m is actually maximal for stable operation of the accelerator. The proposed correct energy of the beam after one accelerating section is about 65 MeV. In this case, the field strength in the first cell will be below 40 MV/m (about 35 MV/m), but acceleration rate – 21 MeV/m. Taking into account imperfection of the structures, realistic rate of acceleration will be ≈17 MeM/m. If interval between the sections is 1 meter, then one accelerating module will occupy 7 m and provide the energy of 102 MeV. Fig. 4.52 represents a sketch of the BINP-developed accelerating structure.

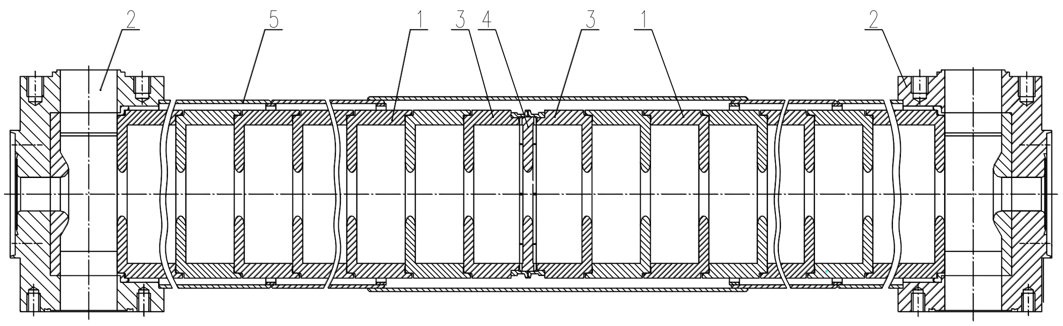

Fig. 4.52. Accelerating structure: regular accelerating cell (1), transformer of a wave-type (2), transitive (connecting) accelerating cell (3), connecting diaphragm (4), cooling jacket (5).

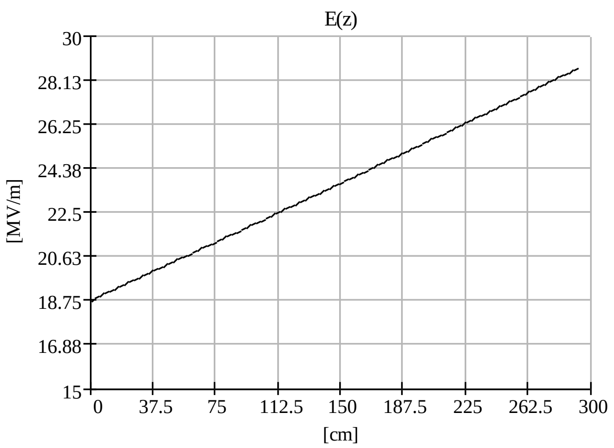

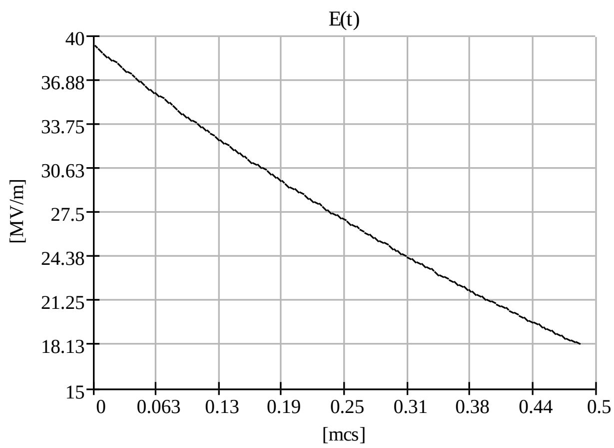

Fig. 4.53. Distribution of electric field strength along the structure (at the left) and dependence of electric field strength in the first cell on time (at the right).

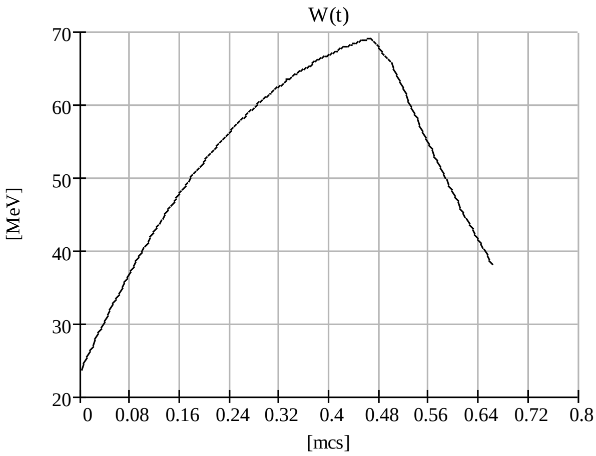

Fig. 4.54. Energy gained by a beam vs time of injection into the AS (time is counted after phase reversal in SLED system)

4.4.2. Beam focusing system

After the sub-harmonic cavity, there is the electron beam longitudinal compression, at which Coulomb repulsion force increases. Thus, the beam should move in increasing axial magnetic field. Such field can be obtained, for example, by means of the rings with current. Their supposed view and field distribution are represented in Fig. 4.55 and Fig. 4.56, respectively.

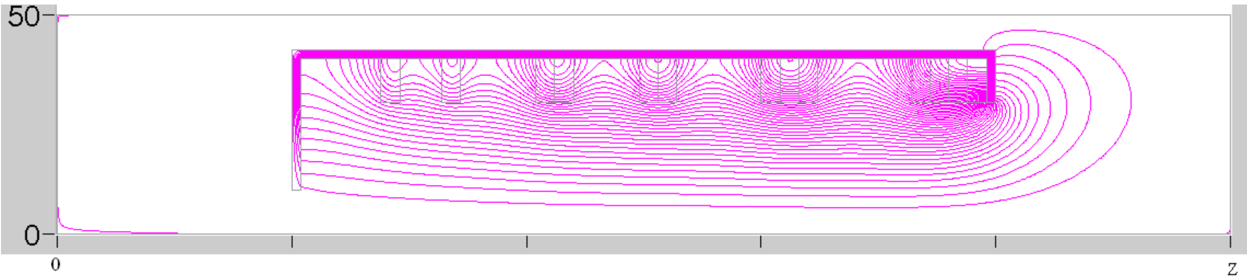

Fig. 4.55. Rings with current and the distribution of magnetic field lines.

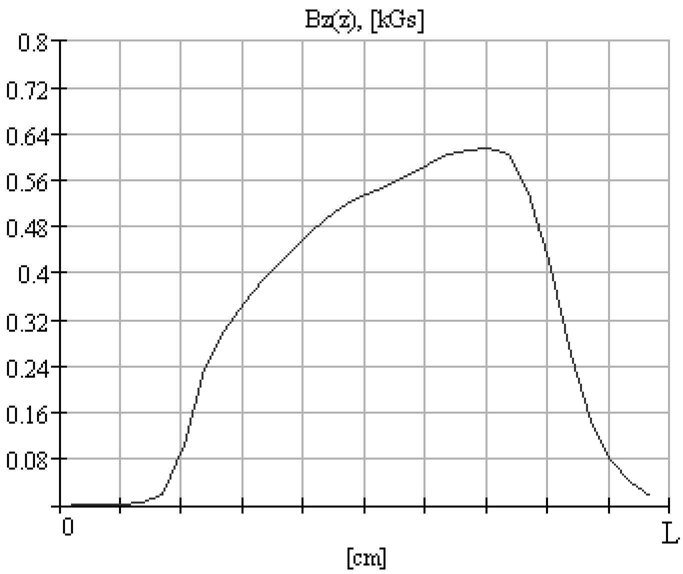

Fig. 4.56. Distribution of magnetic field of the rings with current.

At passing the first accelerating structure, the beam should move in magnetic field of solenoid. The solenoid is desirable to be iron-free to provide a "softer" injection of the beam into the structure. Calculation of particle dynamics should determine the field value, the preliminary value is not more than 3 kGs.

4.4.3. RF load

BINP-developed cavity RF load consists of two low-Q cavity structures connected with a rectangular waveguide (cross-section - 72×34 mm) through the apertures in a wide wall. Plunger is placed at the end of the waveguide, opposite the entry. The distance between the connection apertures and the plunger corresponds approximately to half-length of electromagnetic wave in the waveguide. The magnetic field from the side of supplying waveguide and inside each cavity assemblage around the connection apertures has the maximum value. Usage of two connection apertures allows the raise of electric strength of the structure due to the decrease of electric field strength on the aperture surface and the decrease of the average power level dissipated at each aperture. The operation mode for each assemblage is analogous to mode E_{020} of the cylindrical cavity. The general view of the load is shown in Fig. 4.57.

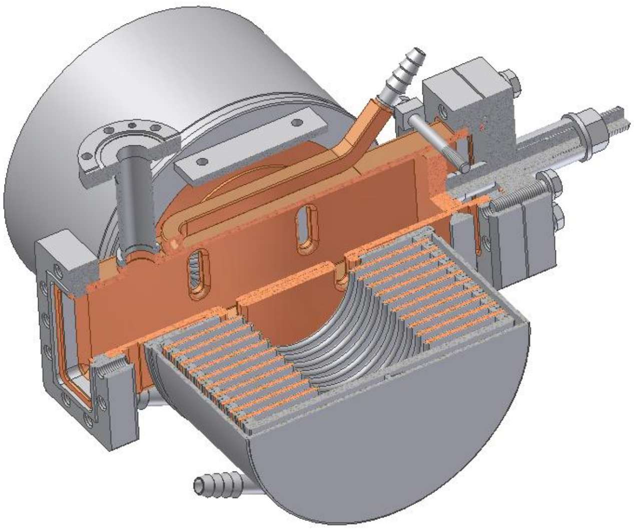

Fig. 4.57. Design of the load for the maximum pulse and average power.

The main parameters of RF loads of three types are represented in Table 4.11.

Table 4.11. Main parameters of RF loads.

Load type	Low	Average	High
Level of absorbed power (MW)	1	60	120
Cavity diameter (mm)	180	182	184
Aperture size (mm)	39	39	39
Cavity height (mm)	5	5	5
Disk thickness (mm)	-	5	5
Quantity of cavities in assemblage	1	5	11
Bandwidth at SWRv level of 1.21 (MHz)	2.2	2.5	2.5
Loaded Q factor	200	180	180

4.4.4. Conclusion

The basic element of the linear accelerator is the accelerating module of 7-m length. For a stable operation mode the acceleration gradient is desirable to be about 17 MeV/m. In this case, the gain of beam energy after such module will be 102 MeV. To gain the energy of 2 GeV, 20 modules with total length of 140 m are necessary. For the energy of 500 MeV, 5 modules and 35-m length are necessary. Besides, the bunching system with a free interval of about 1.5 m should be placed between the source of polarized electrons and the first accelerating section. The schematic view of the electron accelerator to energy of 500 MeV is represented in Fig. 4.58.

Positrons come to the accelerator from the pre-injector with 500-MeV energy, therefore, they should be accelerated up to energy of 2 GeV (Fig. 4.59).

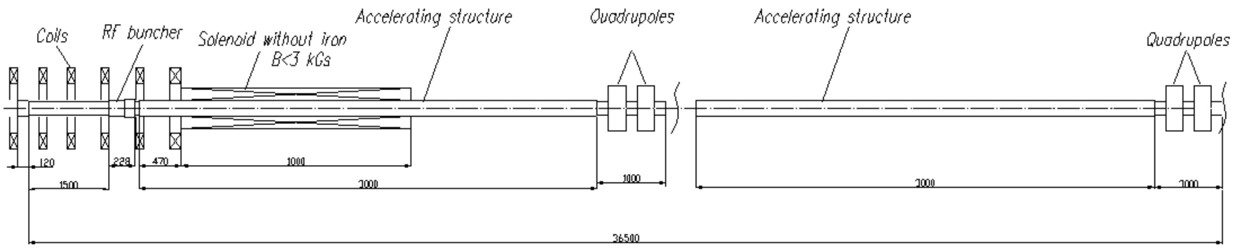

Fig. 4.58. Schematic view of the beginning of the electron accelerator.

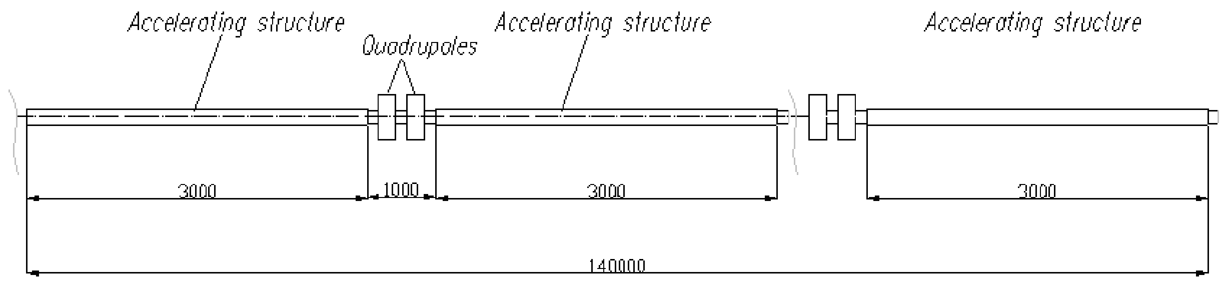

Fig. 4.59. Schematic view of 2-GeV accelerator.

References

1. R.Chehab. Positron Sources. Proc. CERN Accelerator School, General Accelerator Physics, Geneva, 1994, p.643
2. H.-H. Braun “Positrons for Accelerators”, Ph.D. thesis, Zurich University, 1992.
3. D. Yount and J. Pine “Production of Positrons with the Stanford Mark III accelerator”, Nucl. Inst. and Meth. 15, pp 45-50, 1962.
4. A.A.Kulakov, P.V.Martyshkin «Development of the positron source on the basis of linear accelerators», BINP preprint № 99-26.
5. A.N.Skrinsky, V.V. Parchomchuk «Methods of cooling the charged particle beams», Physics of elementary particles and atomic nucleus, 1981, vol. 12, ed. 3.
6. R. H. Helm, “Adiabatic Approximation for Dynamics of a Particle in the Field of a Tapered Solenoid”, SLAC-4, 1962.
7. G.Knopfel. Superstrong pulsed magnetic fields. "Mir", Moscow, 1972.
8. [Lapik2001] R.Lapik, P.Martyshkin. Capture Efficiency of High Field Flux Concentrator. PAC-2001, 2001.

9. C. Leroy, P.-G. Rancoita. Principles of Radiation Interaction in Matter and Detection. World Scientific, 2004
10. The Stanford two-miles accelerator. Ed. by R. B. Nearl, New-York-Amsterdam: W. A. Benjamin, Inc. 1968.
11. R. Chehab, G. L. Meur, B. Mouton, M. Renard. An adiabatic matching device for the Orsay linear positron accelerator. LAL/RT/83-03 March 1983.
12. S. Ecklund, Positron Target Materials Tests, SLAC-CN-128, 1981 г.
13. M. Borland, “elegant: A Flexible SDDS-Compliant Code for Accelerator Simulation”,
14. Advanced Photon Source LS-287, September 2000.
15. Klaus Gruppen «Detectors of elementary particles», Novosibirsk 1999
16. http://cern.ch/geant4
17. R. Pitthan et al., “SLC Positron Source-Simulation and Performance”, IEEE Particle Accelerator Conf., San Francisco, CA, 1991, in Particle Accel.Conf: IEEE 1991:2098-2100 (QCD183:P3:1991).
18. HIGH-YIELD POSITRON SYSTEMS FOR LINEAR COLLIDERS. By J.E. Clendenin (SLAC), SLAC-PUB-4743, April 1989. Published in Proceedings of the 1989 Particle Accelerator Conference, March 23 - 27, 1989, Chicago, IL. p. 1107.
19. RECENT IMPROVEMENTS IN THE SLC POSITRON SYSTEM PERFORMANCE. By P. Krejcik, W.J. Corbett, Stanley D. Eeklund, P. Emma, T.H. Fieguth, Richard H. Helm, A.V. Kulikov, T. Limberg, H. Moshammer, M.C. Ross, R. Siemann, W.L. Spence, M.D. Woodley (SLAC). SLAC-PUB-5786, Mar 1992.3. Contributed to 3rd European Particle Accelerator Conf., Berlin, Germany, Mar 24-28, 1992.
20. Abe, et. al., “The KEKB injector linac”, Nucl. Instr. and Methods A, Vol. 499, pp. 167-190 (2003).
21. T. Kamitani, et. al, KEKB INJECTOR LINAC STATUS AND FUTURE UPGRADE, Proceedings of EPAC 2002, Paris, France
22. Sannibale, et al, DAΦNE Linac Commissioning Results, Frascati, April 4, 1997. Note: BM-2.
23. R. Boni, F. Marcellini, F. Sannibale, M. Vescovi, G. Vignola: "DAFNE Linac Operational Performances", Proceedings of the European Particle Accelerator Conference, Stockholm (Sweden), 22-26/6/1998, p. 764.
24. M.A. PREGER, et al., PERFORMANCE AND OPERATION OF THE DAFNE ACCUMULATOR, Proceedings of the European Particle Accelerator Conference, Stockholm (Sweden), 22-26/6/1998, p. 415.
25. X. Yu, Y. Chen, X. Wang, M. Liu, OPERATION STATUS OF THE BEIJING ELECTRON-POSITRON COLLIDER, Proceedings of APAC 2004, Gyeongju, Korea
26. G. X. Pei et al., Design Report of the BEPCII Injector. Linac, IHEP-BEPCII-SB-03-02, November 2003.
27. J. Clendenin, et. al., “Compendium of Scientific Linacs”, CERN/PS 96-32 (DI), 1996
28. A. Frebel and G. Hemmie, “PIA, the Positron Intensity Accumulator for the PETRA Injection”, IEEE Transactions on Nuclear Science, Vol. NS-26, No. 3 (June 1979).
29. New optics of the LEP injector linac for positron production. C. Bourat, H. Braun, L. Rinolfi (CERN) . Jun 1994. Prepared for 4th European Particle Accelerator Conference (EPAC 94), London, England, 27 Jun - 1 Jul 1994. Published in London 1994, EPAC 94, vol. 1, 704-706
30. Alexander Wu Chao, Maury Tigner. Handbook of accelerator physics and engineering. Singapore: World Scientific, 1999
31. Kolomensky A, Lebedev A. Theory of cyclic accelerators. Moscow: PhysMathLit, 1962
32. Sands M. The physics of electron storage rings. An introduction. SLAC, 1979
33. Brook G. Cyclic charged-particle accelerators. Moscow: AtomIzdat, 1970

34. Burshtejn E. L, Voskresensky G.V. Linear accelerators of electrons with intensive beams. Moscow: AtomIzdat, 1970
35. Wangler T. Principles of RF Linear Accelerators. New York: John Wiley & Sons, 1998
36. R.M.Lapik, P.V.Martyshkin, S. V.Shijankov, A. M. Jakutin. System of the elektron-positron conversion of the VEPP-5 injection complex. BINP preprint №2005-50
37. R. M. Lapik, P. V. Martyshkin. The Capture Efficienty of High Field Flux Concentrator. Proceedings of the 2001 Particle Accelerator Conference
38. A. A. Kulakov, P. V. Martyshkin. VEPP-5 Positron Source Simulations. Proceedings of the 1996 European Particle Accelerator Conference
39. L.D.Landau, E. M.Lifshits. The theoretical physics. T.1 Mechanics. Moscow: "Science", 1988
40. Yu. B. Bolkhovityanov et al., SPIN96 Proceedings, 4, 700 (1997).
41. B.L.Militsyn. “A pulsed polarized electron source for nuclear physics experiments”, Proefschrift (Ph.D. Thesis), Universiteit Eindhoven, Eindhoven (1998).
42. I.Koop et al. “Polarized electrons in AmPS”, NIM-A427, 36-40 (1999).
43. B.L.Militsyn et al., “Beam optical system of the polarized electron source of the Amsterdam pulse stretcher AmPS”, NIM-A427, 46-50 (1999).
44. I.A.Koop. “Longitudinally polarized electrons in AmPS storage ring”, doctoral thesis, Novosibirsk, 2000.
45. L.G.Gerchikov, SPU, St.Petersburg, Russia. “Optimization of Semiconductor Superlattice for Spin-Polarized Electron Source”, PESP2008 - workshop on sources of polarized electrons and high brightness electron beams.
46. M.Yamamoto, Nagoya University. “High polarization and low emittance electron source for ILC”, CCAST workshop on TeV physics and the LHC, Beijing, 2006.
47. F.Furuta et al., NIM-A 538(2005), 33-44.